Impacts of Forest Loss on the Global Water Cycle of the Permian-Triassic Extinction

by

Garridan Porter

Submitted in partial fulfillment of the requirements for the degree of Bachelor of Science in Earth Science

at

Dalhousie University

Halifax, Nova Scotia

April 2022

Supervisor: Dr. Shannon Sterling

Table of Contents

Abstract

Recent studies have shown profound effects of deforestation on decreased precipitation and evapotranspiration. This can be attributed to the concept of green water, which is the volume of water stored in soils and interacting with plants via evapotranspiration. The Permian-Triassic (P-T) extinction had the most profound impact on plant life of any mass extinction, with many large forests being replaced by herbaceous lycophytes. The aim of this study is to explore a large-scale extreme example of deforestation by analyzing the green water variables of the Permian-Triassic extinction linked to the global loss of Glossopteris and related forests. When exploring this event, two main questions are focused on; how did the global distribution of green water differ after the extinction, and how could these alterations have affected global climate at the time? To answer these questions, variables from various studies are transferred into ArcPro and used to make first estimates of seasonal evapotranspiration, latent heat flux, and mean residence time before and after the P-T extinction. Results show a decrease in all water balance variables after the P-T and a correlation between areas of higher decrease and pre-extinction forests. When evapotranspiration change is converted to a change in sensible heat, a global change of approximately 2^{o}C is observed, accounting for approximately one fifth of the post-extinction temperature increase.

Keywords: Water Balance, Permian-Triassic Extinction, Evapotranspiration, Deforestation, Sensible Heat

Glossary

Actual Evapotranspiration - The amount of evapotranspiration that would occur in given conditions of soil, vegetation, and climate, normalized to the amount of water present (Thornthwaite, 1948).

Blue Water - The proportion of terrestrial water stored in open and subterranean bodies of water including rivers, lakes, groundwater aquifers, etc. (Sterling, 2019).

Budyko Curve - Originally developed by Mikhail Ivanovich Budkyo and published in 1974, this curve is used to predict actual evapotranspiration from precipitation and potential evapotranspiration based on the optimization of plant life. Areas to the left of the curve define humid environments in which energy (or ET) is the limiting factor. Areas to the right of the curve denote arid climates where water availability becomes the limiting factor (Creed et al., 2014).

Green Water - The proportion of terrestrial water stored in and/or accessible to plant life. This includes water stored in the root zone and water taken in via interception. (Sterling, 2019).

Latent Heat Flux - The amount of energy required for the conversion of liquid water to vapour during evapotranspiration (Denning, n.d.)

Mean Residence Time - The amount of time a parcel of water will spend in a catchment area. It is calculated by finding the total amount stored in the catchment area and dividing by the rate of flux (Sterling, 2019).

Potential Evapotranspiration - The amount of evapotranspiration that would occur in given conditions of soil, vegetation, and climate, assuming that water availability is not a limiting factor (Thornthwaite, 1948).

Water Balance - The sum of input and output variables that define a hydrologic system, typically including evapotranspiration, precipitation, and runoff (with or without groundwater influence) (Sterling, 2019).

Acknowledgements

I would like to personally thank my supervisor, Dr. Shannon Sterling, for their guidance and support throughout the development of this thesis, as well as Dr. Chris Greene for support with the ArcPro component of this project. Thanks is also given to Dr. Tarah Wright for coordinating the honours program and providing valuable support throughout this project. An extended thanks is given to the faculty of the Dalhousie Earth and Environmental Science Department, for providing the knowledge needed to undertake this project and for continued support throughout my years at Dalhousie University. Lastly, I would like to thank my family and friends who provided support this past year and encouraged my passion for the field of earth science.

1 Introduction

1.1 Problem Statement

Deforestation has become a growing concern in many regions in recent years. On a global scale, between 1992 and 2018, 438 Mha of terrestrial forest cover has been converted to a different land cover type, mainly for agricultural use (Hu et al., 2021). Deforestation can have profound effects on terrestrial water stores, since forest loss can result in the loss of soils layers which act as a store of surface water (Cook et al., 2012). Studies in the Amazon have linked deforestation in the region to decreases in precipitation and localized increases in temperature (Nobre et al., 2009). Further studies in this area have found correlations between forest loss, increased runoff, and decreased evapotranspiration (Guimberteau et al., 2017). All of these factors greatly increase the aridity of the region and cause further damage to the local ecosystem (Cook et al., 2012). Efforts have therefore been made to model impacts of widespread global forest loss, including impacts on regional and global climate (Hu et al., 2021). This study will analyze an extreme deforestation event by applying modern water balance equations to the global loss of forests during the Permian-Triassic extinction. In doing so, the first approximations of Permian-Triassic water balance will be derived.

1.2 Background

1.2.1 The Permian-Triassic Extinction

The P-T extinction had the greatest impact on life of any of the five major extinction events in Earth's history. The extinction occurred at the Permian-Triassic boundary approximately 251.9 million years ago, coinciding with the initial breakup of the supercontinent Pangaea (Cui et al., 2021). Based on a rarefaction analysis, the marine extinction rate was greater than 90% (Erwin, 1994). Recent analyses of marine data have shown that during the time of the extinction, the surface of the ocean was heated to lethal temperatures, while the deep ocean became highly anoxic and sulfidic (Song et al., 2014). There remained a small refuge zone between these two layers that allowed some specifically adapted organisms to survive (Song et al., 2014). While the effects on terrestrial life were still quite devastating, it was less severe than the impact

on oceans with a 75% extinction rate for vertebrate fauna (Erwin, 1994). Despite this lower percentage there were some noticeable groups lost. Paleosediments from after the extinction show very little or no bioturbation, indicating a loss of major soil-dwelling organisms (Buatois et al., 2021). Furthermore, the P-T extinction had the most profound impact on plant life when compared to all other mass extinctions (Cascales-Miñana et al., 2015). It has been noted that almost all major groups of modern plants showed up in the fossil record after the P-T extinction caused the loss of many of the plant groups from the Paleozoic (Cascales-Miñana et al., 2015). Given the dramatic impact of the P-T extinction on Permian flora and fauna, a powerful driving force must have initiated this event.

Multiple theories as to the cause of the P-T extinction exist, with a predominant focus on the similarly timed Siberian Trap eruption (Cui et al., 2021). Geochemical data suggests that there were three phases of eruptions originating in the northern region of what is now Siberia (Burgess et al., 2017). The area covered by the Siberian traps reached a total of 3.46 Mm making it one of the most significant large igneous provinces in geologic history, although larger areas have been recorded (Park et al., 2021). These expansive volcanic sills came into contact with organic sediments, baking them and causing the release of large volumes of carbon dioxide into the atmosphere (Burgess et al., 2007). The eruptions also led to increased carbonate erosion in the surrounding areas, producing higher levels of carbon dioxide (Payne & Kump, 2007). In total, an estimated 10^18 mol of carbon was released in a timespan of less than 20,000 years (Payne & Kump, 2007) and atmospheric pCO_2 increased by 13% (Cui et al., 2021). This carbon increase has also been noted using carbon-13 isotopes from plant fossils, showing a spike in atmospheric CO_2 at the time of the extinction (Wu et al., 2021). The temperature increase caused by this sudden massive carbon release would have triggered a chain reaction methane release by melting permafrost and weathering shelf sediments rich in methane-hydrates (Brand et al., 2016). Measurements taken from both biotic and abiotic sources dating to the late Permian show two major pulses of methane emission (Brand et al., 2016). This combination could have been the key to pushing an already greenhouse state earth into the extreme conditions required for the outcomes seen in this extinction. Phanerozoic temperature ranges have been compared

to the timing of large igneous provinces such as the Siberian Traps, and it has appeared there has been a correlation between these major eruptions and significant increases in global temperatures (Scotese et al., 2021). The Siberian Trap theory is not without scrutiny however, as studies comparing the extent of large igneous provinces and global ice sheet extent have suggested that in similar large-scale eruptions, there is not an impact substantial enough to push the climate to the extremes seen in the P-T extinction (Park et al., 2021). The amount of carbon expelled into the atmosphere from this event would have had dramatic impacts on global climate.

Aside from carbon dioxide and methane, alterations in other atmospheric molecules have been recovered using various methods. Pollen samples from the time of the extinction show evidence of increased acid precipitation (Black et al., 2014). This is further supported using oceanic chemostratigraphy, which shows not only elevated methane levels during the late Permian, but also increased levels of sulfur and nickel (Saitoh & Isozaki, 2020). This significant increase in nickel levels could have been detrimental to the plant life at the time (Saitoh & Isozaki, 2020). Pollen samples from the time of the P-T extinction have also been found across the globe with similar mutations typical in pollen exposed to high levels of solar radiation (Beerling, 2007). Analysis done in some samples of pollen from this period suggest that atmospheric levels of ozone had also dropped during the extinction (Black et al., 2014). It is possible that during this time, the increase in methane and hydrogen sulfide, coupled with the loss of oxygen due to the loss of major producers, led to a major reduction in the earth's ozone layer, causing elevated levels of solar radiation to bombard the earth's surface (Beerling, 2007). There is some counter-evidence to this proposed ozone loss model. The SCION model was used to show the atmospheric element trends throughout geologic history, and while it does agree with the elevations in carbon dioxide and support elevated temperatures, it suggests that the percentage of O2 in the atmosphere leveled out and remained consistent through the Permian and into the Triassic (Mills et al., 2021). Multiple theories as to the cause of the events leading to the P-T extinction have strong supporting arguments, and it is therefore likely that the extinction was the sum of multiple input events. If so, a combination of these theories could prove to be the correct

interpretation and lead to the observed results. However, to date no definitive model for the cause of the P-T extinction has been established.

1.2.2 Climate During the P-T Extinction

Various climate and hydrologic variables have been determined for the P-T extinction, and in some cases have associated spatial data across the supercontinent of Pangaea. Due to the nature of the Permian landmass as one large continent, the climate zoning at the P-T boundary was quite different in some areas than what is observed today (Kutzbach & Ziegler, 1993). Furthermore, Pangaea existed in a greenhouse climate, meaning the temperatures at the poles were not below 0^{o}C for the entire year (Kiehl & Shields, 2005). During the northern hemisphere winters, the North Pole would reach temperatures around -5^{o}C, and during the summers would reach temperatures around 10^{o}C (Kiehl & Shields, 2005). The South Pole saw the opposite pattern, reaching around 5^{o}C in the northern hemisphere winters and around -20^{o}C in the summers (Kiehl & Shields, 2005). After the extinction, temperatures across Pangaea rose by around 10^{o}C, leading to a further shift to greenhouse conditions at the poles (Scotese et al., 2021). The center of the continent contained two large hotspots that would alternate between the 30^{o} North and South latitudes in northern summers and winters respectively (Kiehl & Shields, 2005). These hotspots were associated with low amounts of seasonal and annual rainfall before the extinction (Kutzbach & Ziegler, 1993). This hotspot trend continued even after the P-T extinction (Chandra et al., 2021). These hotspots also correlated with regions of low soil moisture in the center of Pangaea (Kutzbach & Ziegler, 1993). These climate zones meant that the deserts and savanna-like environments of Pangaea would have been concentrated around the 30^{o} North and South latitudes (Kutzbach & Ziegler, 1993). The forests of Pangaea would have been concentrated between these two latitudes, and also extend north and south towards the poles of the continent (Kutzbach & Ziegler, 1993). This allowed much of Pangaea before the extinction to be dominated by tropical and temperate forests.

1.2.3 Permian to Triassic Flora

Before the P-T extinction a lot of the earth was dominated by large tropical forests. One of the most predominant of these large trees was the morpho-genus

Glossopteris, a gymnosperm that dominated almost all parts of Gondwana during the Permian (McLoughlin, 2011). Studies of this plant have placed it in the group of pteridosperms, seed-bearing gymnosperms excluded from the more derived groups such as cycads, ginkgos, and conifers (Delevoryas & Gould, 1977). The average Glossopteris tree was estimated to have been about 12 to 19 metres tall, with a cross-sectional area larger than most modern trees (Miller et al., 2016). However, even larger Glossopteris estimates have placed the tree as capable of growing up to 30 metres tall (McLoughlin, 2011). The root structures of Glossopteris were termed Vertebraria (Neish et al., 1993). These structures were complex with multi-layer tissues and hollow air sacs (Neish et al., 1993). The roots of Glossopteris were quite shallow for a plant of its size, but would cover a large surface area as they grew outwards from the tree (McLoughlin, 2011). The Vertebraria roots have been discovered with associated mycorrhizal fungi networks that would have been mutually beneficial to the surrounding productivity (Harper et al., 2013). The sedimentary layers that Vertebraria have been found in show that these structures were adapted for the tropical swamps of the Permian (Neish et al., 1993). Studies of whole Glossopteris forests have found them to be a very productive environment (Miller et al., 2016). A particular forest studied in Antarctica was found to have a higher number of trees per unit area than many modern forests (Miller et al., 2016). The Antarctic forest indicated a higher biomass than many modern forests as well as net primary production exceeding all modern high latitude forests, nearly equaling many tropical forests (Miller et al., 2016). It is clear from these studies that Glossopteris and similar trees were therefore thriving ecosystems that played a key role in the biosphere during the late Permian.

During the P-T extinction there was a stepwise loss of forests and a replacement with more suitably adapted flora. The loss of Glossopteris forests during the P-T extinction was a global phenomena, observed in geologic formations in Norway (Hochuli et al., 2010), China (Feng et al., 2020), and Russia (Davydov et al., 2021). The most severe impacts during the extinction were in the tropics where Glossopteris forests have been seen to be the best adapted (Davydov et al., 2021). Original observations of the trends in the loss of the forests led to the proposal of a three step sequence (Stevens et al., 2011). The first event was a stepwise series of burst extinctions that eliminated

many plant groups that could not cope with the initial conditions of the extinction (Stevens et al., 2011). This was followed by a rapid loss of many species, and then a third event that wiped out all wetland plant communities (Stevens et al., 2011). The harsh climate conditions after the P-T extinction led to sparse plant life across the globe for 3 million years (Frank et al., 2021). Wetlands, that were once a dominating biome in the Permian, took 10 million years to recover (Cascales-Miñana et al., 2015). Vegetation recovery occurred in phases during and after the extinction (Mays et al., 2020). After the collapse of the Glossopteris forests, there were multiple phases of progressively more stable recovery until a rough ecosystem was able to adapt to the post-extinction conditions (Mays et al., 2020). The loss of the once dominating Glossopteris forests during the extinction opened new ecological niches that would come to be exploited by better adapted successors.

The first flora to take hold after the extinction were lycophytes (Feng et al., 2020). The specific lycophytes that dominated after the P-T were herbaceous, ground-level plants (Feng et al., 2020). Herbaceous lycophytes such as Tomiostrobus were well adapted to the arid climates of the early Triassic (Feng et al., 2020). The root structures of these lycophytes were much smaller, consisting of thin hair-like structures that were able to weave into more rocky surfaces, but only covered a small surface area (Augstein & Carlsbecker, 2018). These new lycophytes were shown to be much more resistant to the harsh climates of the Permian-Triassic boundary. However, their resistance to the conditions also meant they were far less productive than the forests that came before.

1.2.4 Permian-Triassic Fluvial Systems

During the P-T extinction, there was an observed shift from low- to high-energy fluvial systems on a global scale. Studies on the Glossopteris forests of what is now Antarctica indicate a broad range of fluvial, floodplain, and wetland environments that supported these types of trees (Cuneo et al., 1993). The loss of land plants in what is now South Africa led to a shift from low-energy meandering rivers to braided rivers with much higher rates of erosion and flow (Ward et al., 2000). This trend was also observed in geologic formations from China (Zhu et all., 2019). The decrease in vegetation and

increase in fluvial system energy would have had detrimental impacts on the environment. The increased weathering prevented soil formations as there was little time for organic matter layers to build up (Zhu et al., 2019). The loss of soils would have had two major impacts on the climate and ecosystem. The first is that this would continue to expose the sediments to the acidic conditions of the P-T extinction which in turn, combined with the general loss of soils, would have led to the extinction of many soil-dwelling organisms (Buatois et al., 2021). The second was that as the sediments erode it became harder for large vegetation to take hold and prevent these hydrological system changes and areas impacted would have become more arid, eventually shifting into alluvial systems (Zhu et al., 2019). In all areas where these fluvial changes occurred it is therefore likely that these events caused feedback effects that furthered the loss of many Permian forests, and drove the domination of the more resilient lycophytes.

1.2.5 Water Balance and Green Water

Studies have linked present day forest loss and other land cover changes to changes in regional hydrology and climate. General studies of conversion of forested to non-permeable land cover types link a loss in forest cover to a decrease in terrestrial evapotranspiration (Sterling et al., 2013). One study applied the Goddard Institute for Space Studies (GISS) model to analyze trends in climate related to deforestation in Mesoamerica (Cook et al., 2012). The results showed that the loss of these forests amplified regional droughts by reducing seasonal and annual precipitation levels which was correlated with a decrease in atmospheric convective activity (Cook et al., 2012). Later studies would combine multiple models and show that deforestation in the Amazon basin led to decreased evapotranspiration and increased runoff in the region (Guimberteau et al., 2017). The study in the Amazon basin seemed to indicate an increase in precipitation following deforestation, which contradicts the results of the Mesoamerica study (Guimberteau et al., 2017). Furthermore, in areas of clear-cutting, there is decreased canopy coverage which reduces local interception (Oda et al., 2021). This water that has escaped from interception then leads to increased runoff, driving total water storage away from the site of clear cutting (Oda et al., 2021). It is clear then

from these studies that there is a strong connection between plant life and the associated regional hydrologic systems.

The link between forests and water balance can be supported by applying the concept of green water to the systems in question. The concept of blue and green water first arose in the mid-2000s where it was applied to the concept of water resource management (Falkenmark & Rockström, 2006). In this two store model, blue water is defined as water found in rivers, oceans, and other open bodies, as well as groundwater, and green water is defined as water stored in the root zone of plants as well as water involved in evapotranspiration (Falkenmark & Rockström, 2006). More recently, green water has included water that is intercepted by vegetation, as well as general soil moisture and water stored in organic matter (Sterling, 2019). Here it will be defined as the pool of water that can interact directly with the atmosphere, thereby excluding groundwater processes (Sterling, 2019). The concept of mean residence time can also be applied to green water, specifying the average length of time meteoric water remains in terrestrial green water stores (Sterling, 2019). The Soil and Water Assessment Tool (SWAT) has been applied in multiple studies to model green water availability (Schuol et al., 2008). The SWAT model was first published in 1998 as a method of quantifying hydrological processes for watershed management (Arnold et al., 1998). It has since been modified to allow for blue and green water assessment using known influencing factors in both Africa (Schuol et al., 2008) and Iran (Faramarzi et al., 2009). In one specific study done in China, it was found that 69 percent of the total water resources were located in green water stores (Wu et al., 2021). By applying this concept and understanding the prevalence of green water in terrestrial ecosystems, the trends observed between forest loss and water balance seem to have a more direct connection.

1.3 Summary of Knowledge Gaps

As shown in this review, the study of water balance has never truly been applied to the conditions of the P-T extinction. Estimations have been made on precipitation, and have been zoned in areas of high and low values across Pangaea as highlighted in section 2.3. However, the values for evapotranspiration have not been estimated

leaving the interactions between terrestrial and atmospheric water incomplete. Furthermore, although extensive work has been done studying the sedimentology of river beds at the P-T boundary, a true hydrologic study has not been conducted to find the typical river discharges before and after the extinction or how the general storage trends of water changed. Finally, given the studies on deforestation and water loss and its effect on regional climate, it is surprising to find no study has attributed a global loss of water and change in atmospheric water interactions to the 10^{o}C change in temperature predicted at the P-T boundary.

1.4 Study Introduction

The purpose of this study is to describe the global and spatial trends of water balance components before and immediately after the P-T extinction. To provide this description, two main research questions will be analyzed. The first is how did the distribution of green water differ before and after the P-T extinction? We hypothesize that all three components of water balance observed in this study (precipitation, evapotranspiration, and discharge), as well as mean residence time of terrestrial water will decrease after the P-T extinction. In answering this first question, the first predictions of water balance for the P-T extinction will be made. The second research question is how could these alterations of green water globally have affected the climate at the time? We hypothesize that latent heat flux should decrease correlating with a decrease in evapotranspiration, leading to an increase in sensible heat and contributing to global warming.

To make initial estimates of the components of water balance, known palaeoclimate variables will be used as inputs for equations used to define present day water balance. These input variables include temperature, precipitation, soil moisture, and land cover before and after the extinction where possible or applicable, pulled from various sources. The temporal range of this study will go from approximately one million years before the extinction, to one million years after the extinction, ranging from 251-249 Ma. Additionally, seasonal data will be gathered where possible to determine differences in spatial variables in the summer and winter. These variables will be georeferenced into ArcPro and rendered as raster data sets which can then be

subjected to various equations to form maps based on desired outputs. Once values for evapotranspiration, discharge (in this study being used to refer to terrestrial runoff), and mean residence time have been determined pre- and post-extinction, the change in each variable will be found. Lastly, the change in evapotranspiration will be converted to latent heat flux, which through a series of conversions can be used to determine the global temperature change that would occur given the predicted change in evapotranspiration. These changes will then be overlaid with a raster set of pre-extinction land cover types to highlight variable changes between forested and non-forested regions. Since all inputs will be calculated globally the same way, this will account for temperature and precipitation impacts caused by the extinction, and the specific land covers should react in different ways to the changing climate.

2 Methods

2.1 Overview

To answer the research questions of this thesis, water balance components for the P-T extinction must be generated on a global average and as spatial data. A full summary of all inputs and equations is provided in Table 1 and summarized visually in Figure 1. When generating these variables, a few key assumptions will be held throughout this study. The first is that all equations will hold true for palaeoclimates as they would for modern climates. This may be more sensitive for methods such as the budyko curve, which has been generated based on modern plant and climate data, but the variation will be assumed insignificant. The second major overarching assumption is that there is no impact from the poles on terrestrial climate. The world was in a greenhouse phase during the Permian and there was no permanent ice cap at the poles. This greenhouse condition was only made worse after the extinction, further validating the ability to disregard the impact of polar ice on Permian and Triassic climates. The final major assumption is that immediately after the extinction there was an insignificant amount of plant life to affect terrestrial systems, this will allow assumptions to be made for terrestrial conditions post-extinction where they were otherwise unavailable that will be discussed further when analyzing the methods of each output. Once these variables have each been generated, they will be compared with a known pre-extinction land cover map shown in Figure 2 (Kutzbach & Ziegler, 1993). The changes will be correlated to pre-extinction land cover type to find the average raw and percent change values for each variable for each pre-extinction land cover type.

Table 1 *Variables used to predict Permian-Triassic water balance as well as the methods/equations, the sources of data, and assumptions associated with each variable. Variables highlighted with an asterisk indicate a variable that will be predicted for the P-T extinction for the first time in this study.*

Variable	Method	Data Sources	Assumptions
Temperature	Raw Data	Kiehl & Shields, 2005 (raw temperature data) Scotese et al., 2021 (P-T boundary temperature increase)	Consistent temperature increase globally
PET*	Thornthwaite Equation (Thornthwaite, 1948)	Temperature data as above Wu et al., 2013 (length of day based on milankovitch cycles)	Thornthwaite equation holds true in paleoclimate settings
Precipitation	Raw Data	Kutzbach & Ziegler, 1993 (pre-extinction data) Chandra et al., 2021 (post-extinction data)	
Dryness*	Budyko Curve (Budyko, 1974)	PET & Precipitation as above	
AET*	Budyko Curve (Budyko, 1974)	Dryness and Precipitation as above	Budyko equations holds true for dryness index values greater than modern biomes
Soil Moisture	Raw Data	Kutzbach & Ziegler, 1993	
Discharge*	Water-balance (P - ET)	Precipitation and AET as above	
MRT*	Mean Residence Time Equation	Soil Moisture and Discharge as above	Assumes post extinction MRT is 0
Sensible Heat*	Latent Heat Equation	Input the AET values with additional constants	Assumes a decrease in latent heat is equal to sensible heat increase
Land Cover	Raw Data	Kutzbach & Ziegler, 1993	All forest land covers post-extinction would be roughly equivalent to the water balance of the desert land cover

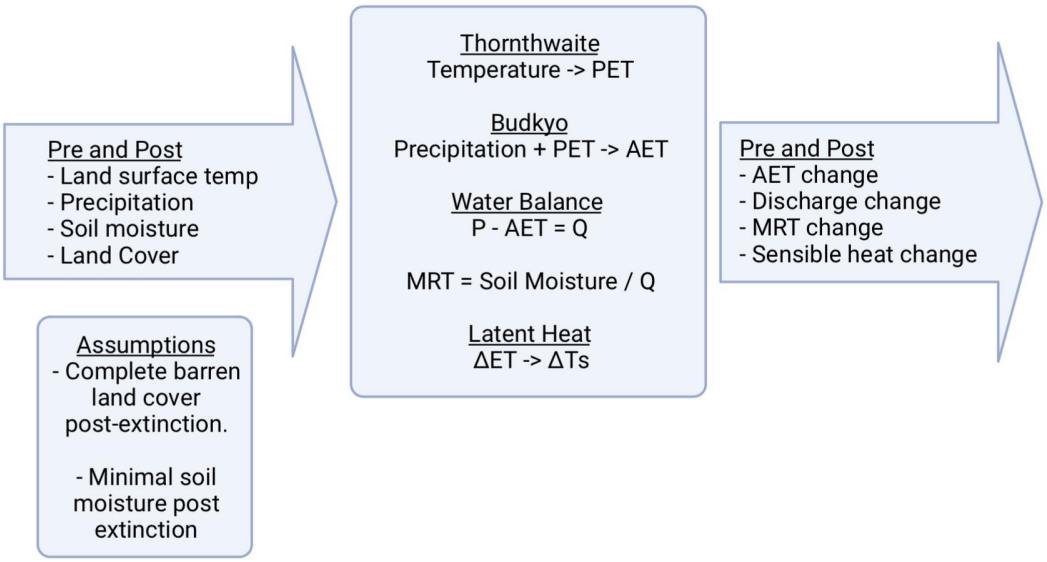

Figure 1 *Summary of input variables, intermediate equations, output variables, and assumptions for the prediction of Permian-Triassic water balance.*

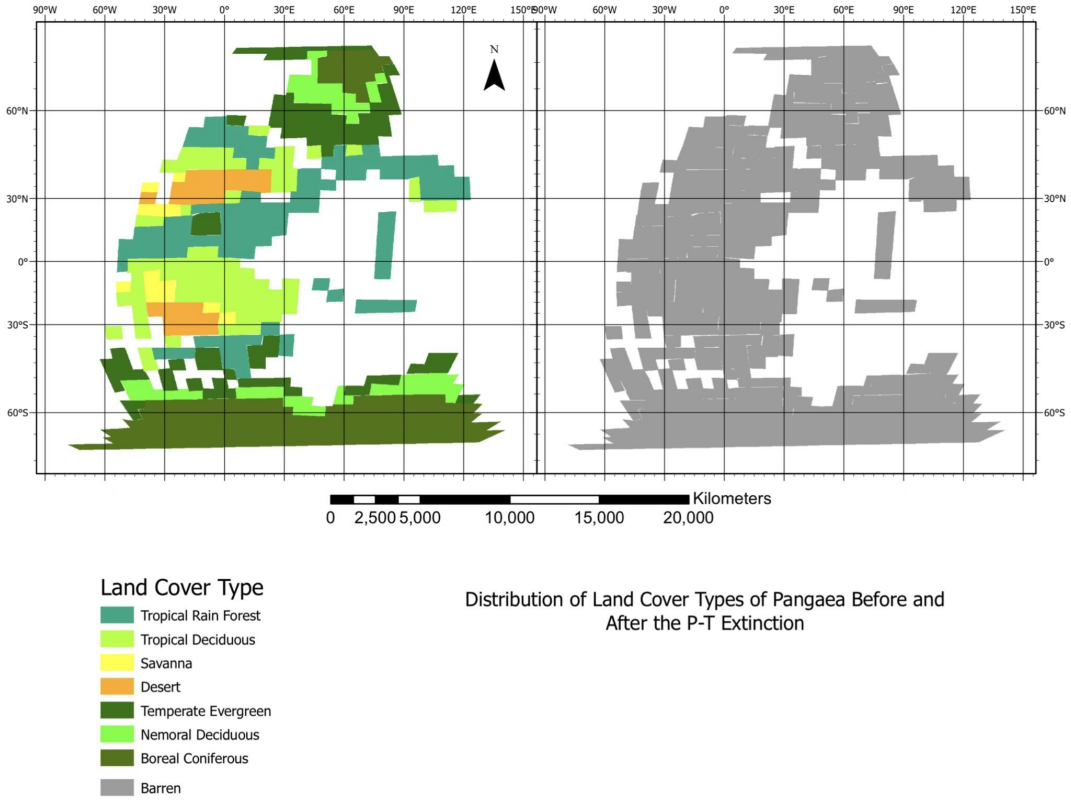

Figure 2 *Land cover types before (left) and after (right) the P-T extinction. The left map is a digitized version of land cover generated by Kutzbach & Ziegler in 1993. The legend variables are pulled from this study. Nemoral deciduous otherwise refers to temperate deciduous. The right map shows a single barren land cover signifying an absence of plant life and assumed arid nature, but not holding to precipitation limitations of a desert environment.*

2.2 Water Balance

The components of water balance were all derived from initial estimates found for temperature and precipitation before and after the P-T extinction. The two main starting input variables (temperature and precipitation) were digitized into maps seen in figure 3, 4 and 5. Although no temperature maps were available for post-extinction data, known temperature changes at the P-T boundary (Scotese et al., 2021) could be applied to transform the pre-extinction data into post-extinction data, assuming that the zones of high and low temperature did not vary significantly after the extinction. It is important to note that these variables come from multiple studies and therefore have slight variations in the configuration of the continents, meaning some areas in the final predicted water balance variables will be undefined. A raw change calculation was also applied to the precipitation map to get a prediction of change in precipitation at the P-T boundary (figure 6). Using the generated maps, raster calculations were applied to generate variables as outlined in section 3.1. The generation of variables began by using the Thornthwaite equation to convert temperature to potential evapotranspiration (PET). This could then be interpreted alongside precipitation using the Budyko curve to get an estimate of actual evapotranspiration (AET). Once precipitation and evapotranspiration were known, a mass balance formula could be used to find discharge. The last calculation for mean residence time would define the storage of the system divided by the discharge. This sequence gives the full set of water balance variables and will be expanded on in the following two sections.

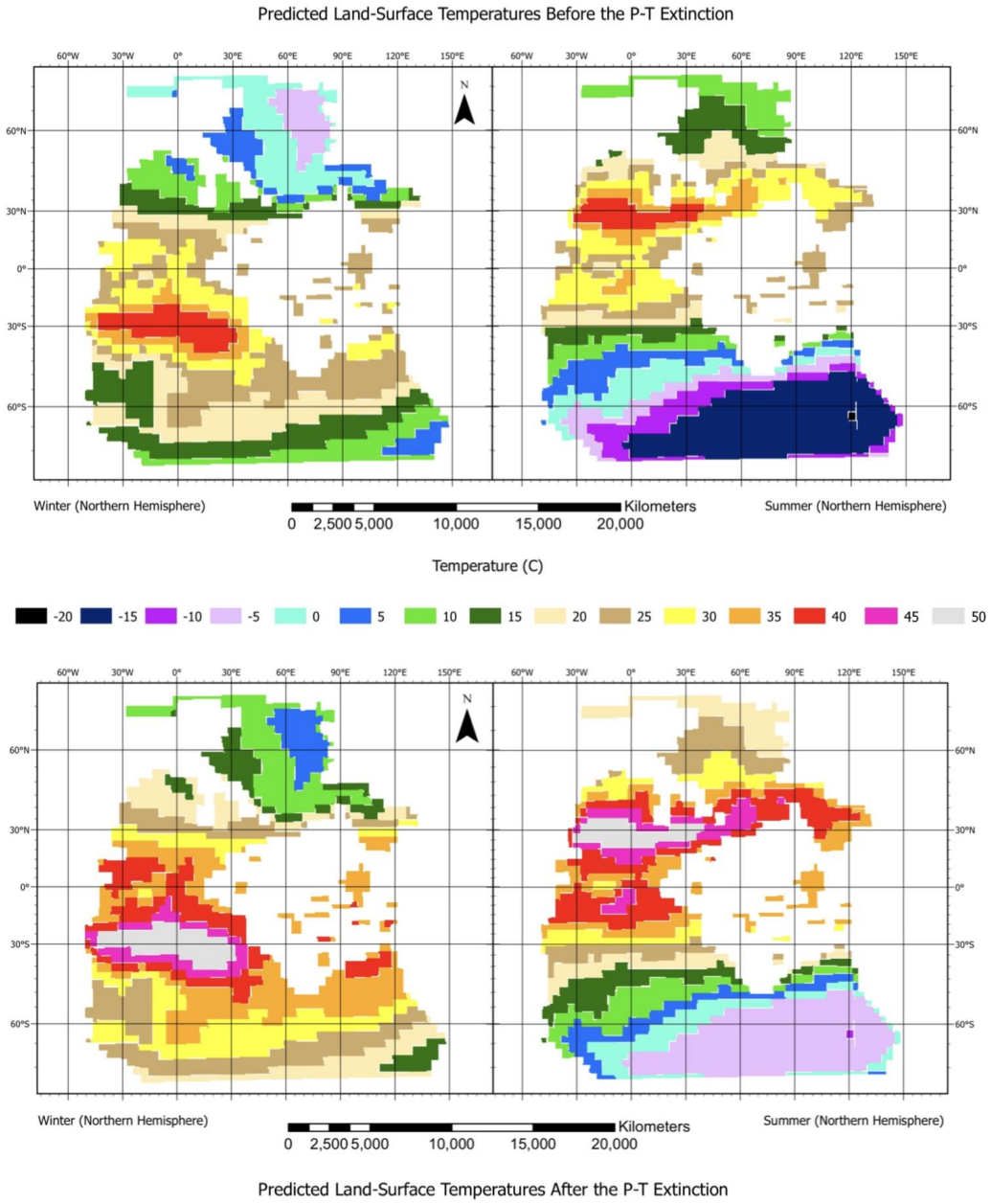

Figure 3 *Maps of predicted seasonal temperature values for Pangaea before (top) and after (bottom) the P-T extinction. The pre-extinction temperatures are digitized from a previous study (Kiehl and Shields, 2005). The post-extinction temperatures had a global increase applied from known temperature curves of 10°C (Scotese et al., 2021). The seasons are based on northern latitudes.*

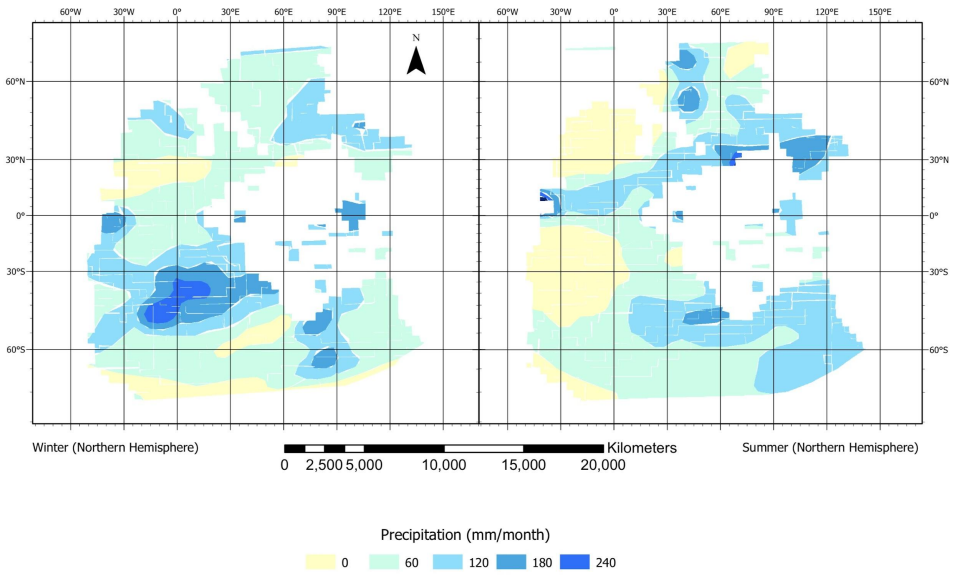

Predicted Precipitation Before the P-T Extinction

Figure 4 *Predicted seasonal terrestrial precipitation for Pangaea before the Permian-Triassic extinction. Original precipitation values derived from Kutzbach & Ziegler, 1993, and clipped to show only precipitation data over the supercontinent of Pangaea. The seasons are based on northern latitudes.*

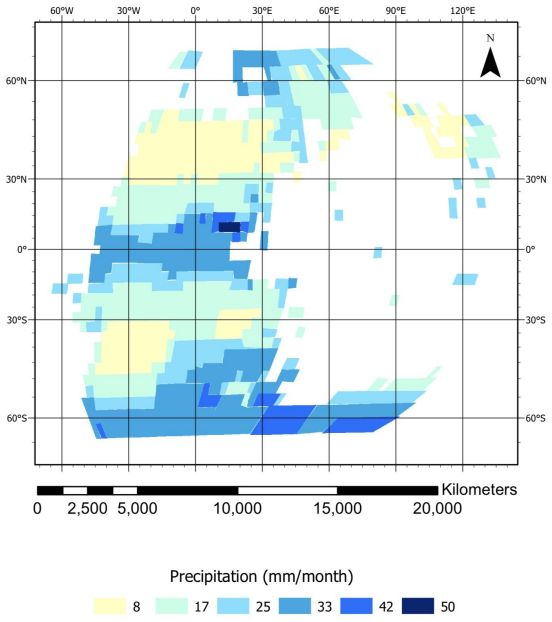

Predicted Precipitation After the P-T Extinction

Figure 5 *Predicted terrestrial precipitation for Pangaea after the Permian-Triassic extinction. Original precipitation values derived from Chandra et al., 2021.*

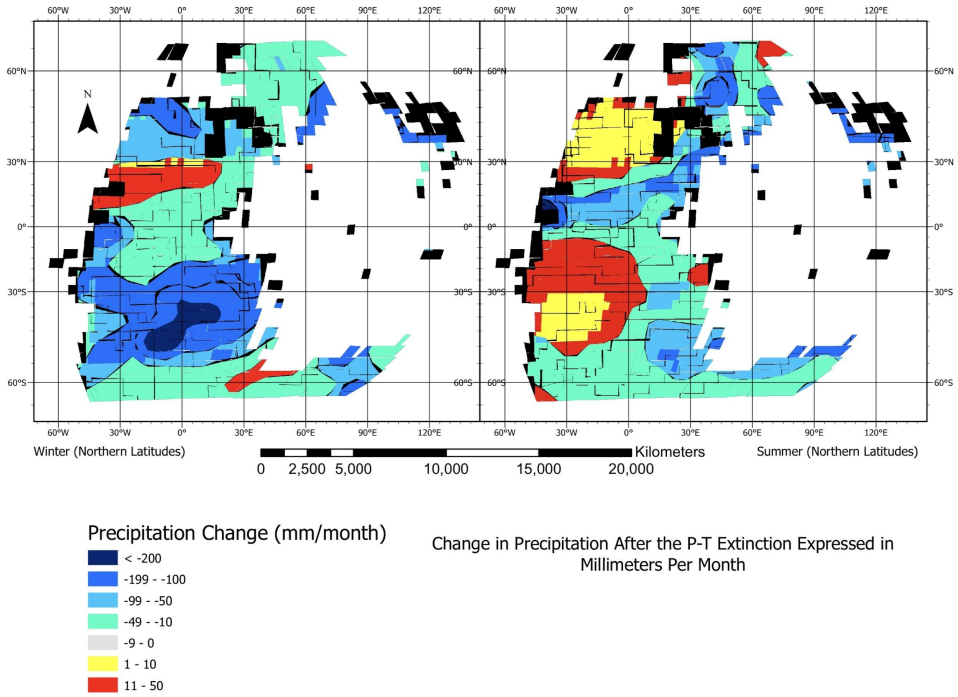

Figure 6 *Maps of change in precipitation after the P-T extinction for northern latitude winter and summer. Change in precipitation is expressed as raw change in millimeters per month. Zones in black indicate areas where temperature zones were negative or where land mass assumptions from different studies did not overlap and are therefore undefined. Average loss across the continent was -45.6 mm/month.*

2.2.1 Actual Evapotranspiration

The first step in estimating evapotranspiration was to use the Thornthwaite equation to find potential evapotranspiration. Potential evapotranspiration (PET) is an estimation of the maximum possible values of evaporation and transpiration for a climate condition assuming available water is not a limiting factor (Allen et al., 1998). The Thornthwaite equation (equation 1) correlates number of hours per day and average temperature to find potential evapotranspiration (Thornthwaite, 1948). The Thornthwaite equation has been found to underpredict by up to 48% and is less accurate for highly tropical or arid regions which define much of Pangaea (Moeletsi et al, 2013). The Penman-Monteith model has been established as the recommendation for studies on evapotranspiration modeling (Allen et al., 1998). However, the Penman-Monteith model has many more variables than the Thornthwaite equation, some of which are not possible to obtain for a paleoclimate study. It is also possible to adjust the Thornthwaite equation to closer approximate Penman-Monteith outputs, but

this too requires variables that cannot be determined for paleoclimate work (Ahmadi & Fooladmand, 2008). Therefore, this study is limited to the original derivation of the Thornthwaite equation, which may underpredict the true evapotranspiration values for the P-T extinction. To apply this equation, the number of hours per day were needed for the Permian. This was found to be approximately 22 hours (Wu et al., 2013). The Thornthwaite equation could then be applied as a raster calculator using the temperate maps as an input.

$$PET = 16(L/12)(N/30)((10T_d)/I)^{\alpha} \quad (1)$$

PET = Potential evapotranspiration (mm/month)
T_d = Average daily temperature (^oC)
N = number of days per month (assume 30)
L = Number of hours per day (22)
I = Heat index = $\Sigma(T_{mi}/5)^{1.514}$
T_{mi} = Monthly temperature (^oC)
$\alpha = (6.75x10^{-7})I^3 - (7.71x10^{-5})I^2 + (1.792x10^{-2})I + 0.49239$

Once potential evapotranspiration was found, it could be compared with precipitation to find actual evapotranspiration using the Budyko curve. The Budyko curve was developed by Mikhail Ivanovich Budkyo and published in 1974 and is used to predict actual evapotranspiration from precipitation and potential evapotranspiration (Budyko, 1974). Shown in Figure 7, the curve displays an empirical model of how plant life optimizes available water across a range of global climates (Nijzink & Schymanski, 2022). The curve is split into two halves related to the dryness (potential evapotranspiration over precipitation) of the environment (Creed et al., 2014). The left side of the curve, from dryness 0 until 1, represents areas that are energy limiting (Creed et al., 2014). The bottom left corner of the graph would therefore represent moist tropical environments where available water is at a surplus. The right side of the curve, from dryness 1 until 2, represents areas that are water limiting (Creed et al., 2014). Therefore, the top right of the curve would represent arid deserts where the energy required for evapotranspiration surpasses the amount of water available. Assuming that the optimization of plants has held true since their domination in the Devonian, the Budyko curve can be used to predict actual evapotranspiration for the Permian. There have been some alterations to the formula of the Budyko curve since its proposal

(Lhomme & Moussa, 2016). This study will utilize the original formula postulated by Budyko to avoid needing additional input variables seen in later derivations. This formula is shown in equation 2. Dryness was first calculated by dividing the potential evapotranspiration raster by the precipitation raster. This resultant raster is then used as an input into a raster calculation to find actual evapotranspiration using the Budyko formula.

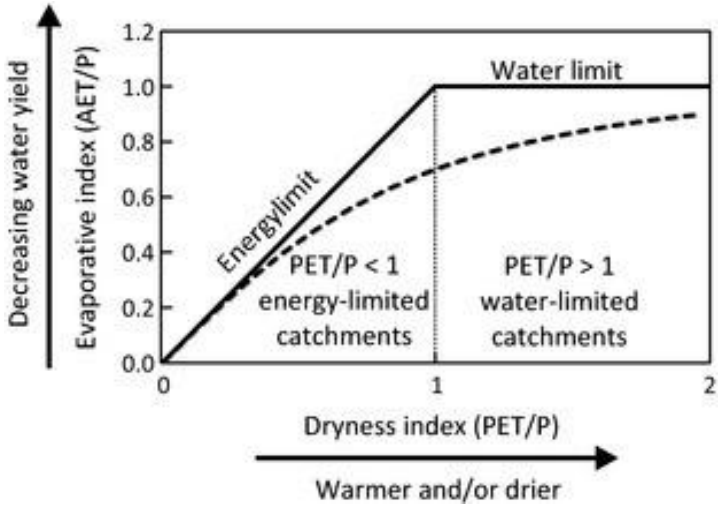

Figure 7 *Budyko curve as depicted in Creed et al., 2014. The solid line indicates the transition from energy limit environments on the left to water limit environments on the right. The dotted line represents the optimized curve of plant life represented by the Budyko equation.*

$$E/P = \{\varphi_p \tanh(1/\varphi_p)[1-\exp(-\varphi_p)]\}^{½} \quad (2)$$

E = Actual evapotranspiration (mm/month)
P = Precipitation (mm/month)
φ_p = Dryness (E_p/P)
E_p = Potential evapotranspiration (mm/month)

2.2.2 Discharge and Mean Residence Time

Discharge, being the last variable needed in the water balance equation, could be calculated by the mass-balance formula. The general mass balance formula for water balance includes precipitation and groundwater as inputs, and evapotranspiration, runoff, and groundwater as outputs. For the context of this study, groundwater will be assumed insignificant. Groundwater can be overlooked as this study focuses purely on

the set of water balance variables that directly interact with the atmosphere, as they would have been most heavily affected during the P-T extinction. Runoff has also been expressed discharge. With these modifications the water balance formula states that discharge would represent the remaining amount of water added by precipitation and not removed by evapotranspiration (equation 3). This formula was used as a raster calculator with AET and precipitation maps as inputs. This leads to zones of undefined areas where negative temperatures cause undefined zones of AET to appear at the poles of Pangaea. However, most of the continent is unaffected by this error.

$$Q = P - ET \quad (3)$$

Q - Discharge (mm/month)
P = Precipitation (mm/month)
ET = Evapotranspiration (mm/month)

Once water balance had been fully calculated, mean residence time could be found by defining storage over flux (equation 4). To define storage, pre-extinction data on soil moisture was found (Kutzbach & Ziegler, 1993). This data was digitized into ArcPro and used to represent the amount of water stored in the terrestrial system (figure 8). No soil moisture data was available for after the P-T extinction so 0 storage is assumed post-extinction. This means that the MRT time before the extinction should see a 100% drop after the extinction. This assumption was made in support of studies that showed extreme erosion events in the P-T extinction prevented soil build up, leaving no organic layers to retain available moisture (Zhu et al., 2019). With storage defined, flux was simply expressed as equal to discharge given that it was the only terrestrial movement of water in the mass balance equation. Equation 4 was then used as a raster calculator function and soil moisture and discharge maps used as inputs to generate MRT.

$$MRT = S/Q \quad (4)$$

MRT = Mean Residence Time (months)
S = Storage (Soil Moisture) (mm)
Q = Discharge (mm/month)

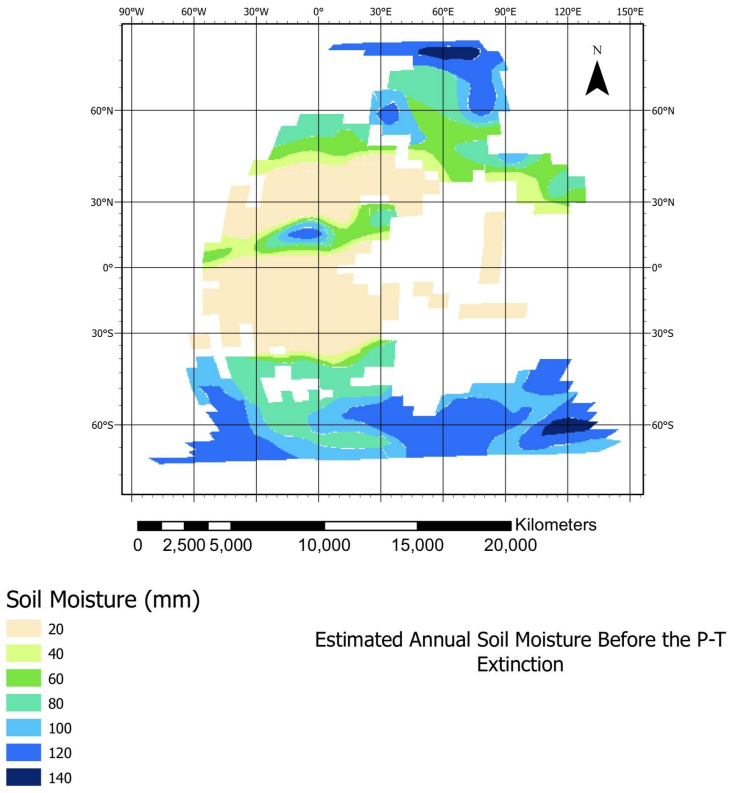

Figure 8 *Predicted soil moisture content for Pangaea before the Permian-Triassic extinction. Original soil moisture values derived from Kutzbach & Ziegler, 1993.*

2.3 Sensible Heat

To find sensible heat, the change in actual evapotranspiration had to be converted into latent heat flux. Latent heat flux defines the amount of energy being used to convert the amount of liquid water being evaporated/transpired into a vapour state (Denning, n.d.). Finding latent heat flux is the first step in converting an evapotranspiration change to a change in temperature. This was used to determine what impact the change in water balance had on the global climate in the P-T extinction. The calculation from evapotranspiration to latent heat flux is shown in equation 5. This formula was applied to a raster calculator with the change in evapotranspiration map representing the Δe variable.

$$LE = (\rho C_p/\gamma)(\Delta e/r) \quad (5)$$

LE = Latent heat flux (W/m^2)
ρ = density of water (constant) ($kg\ m^{-3}$)
C_p = heat capacity of water (constant) ($J\ K^{-1}\ kg^{-1}$)
γ = Psychrometric constant ($Pa\ K^{-1}$)
Δe = change in evapotranspiration (mm/month)
r = aerodynamic resistance (assumed constant) ($s\ m^{-1}$)

The latent heat flux could then be converted from an energy unit, into a unit of temperature. This conversion correlates the amount of work done in evapotranspiration to an equivalent change in temperature. This conversion is done using equation 6. This formula is entered into a raster calculator with the results of equation 5 as the input raster. Once this temperature change is found, the sensible heat change expressed in temperature is equal to the negative of the latent heat flux expressed in temperature, assuming a direct inverse relationship.

$$LE = \rho C_p(\Delta T/r) \quad (6)$$

LE = Latent heat flux (W/m^2)
ρ = density of water (constant) ($kg\ m^{-3}$)
C_p = heat capacity of water (constant) ($J\ K^{-1}\ kg^{-1}$)
ΔT = Change in temperature (^oC)
r = aerodynamic resistance (assumed constant) ($s\ m^{-1}$)

3 Results

3.1 Water Balance

As a global average, there was a decrease in all water balance components after the P-T extinction. Both precipitation and evapotranspiration saw a decrease of one order of magnitude from 1.41e12 to 4.83e11 mm/yr and 1.19e12 to 4.43e11 mm/yr respectively. Discharge showed a much greater decrease of two orders of magnitude from 1.52e11 to 8.42e9 mm/yr. Mean residence time decreased globally by about 50% from 7 months to 3.2 months. These results have been summarized in figure 6.

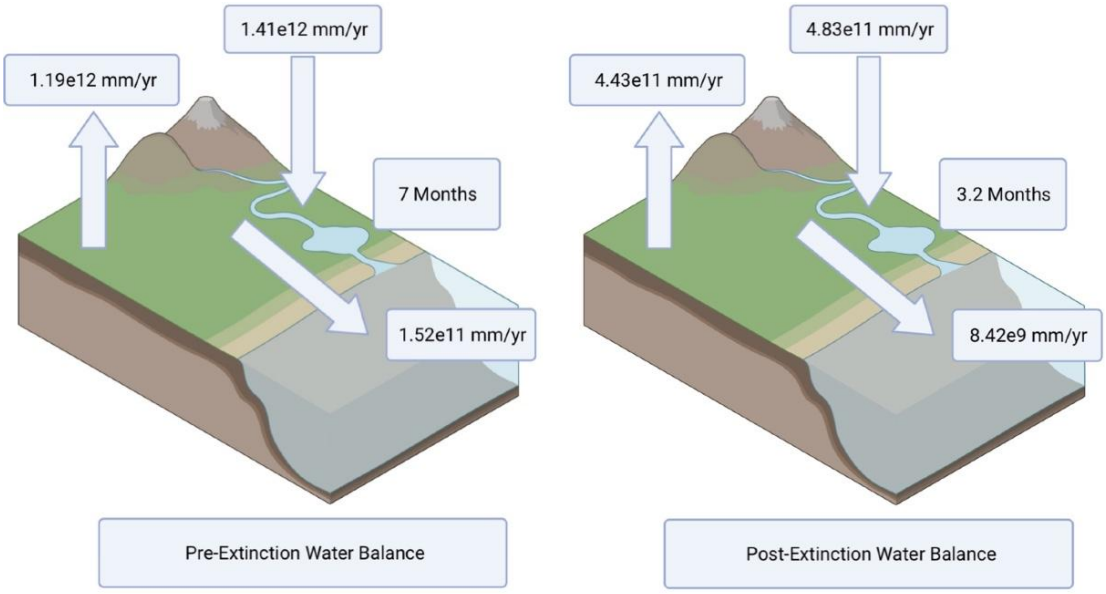

Figure 9 *Global average water balance variables for the supercontinent Pangaea before and after the P-T extinction. Precipitation and evapotranspiration are represented by interactions with the atmosphere, downwards and upwards respectively, and are expressed in mm/yr. Discharge represents the terrestrial runoff and is also expressed in mm/yr. Mean residence time of terrestrial water is expressed as months.*

3.1.1 Actual Evapotranspiration

Estimates of actual evapotranspiration show zones of high and low values that differ by seasons. The pre-extinction values showed much more extreme high and low values. In the winter, the zones of low evapotranspiration are concentrated at the 30° North latitude and the southwestern portion of the continent. The high values are mostly concentrated between the 0° and 60° South latitude. In the summer, the 30° North zone

of low values expands upwards and a new large zone of low values between the 0º and 60º South latitude. The areas of high values sit on a diagonal line stretching from 0º in the west to between 30º and 60º on the eastern side of Pangaea. After the extinction, there were mostly lower values across the whole continent, with only slightly higher values located at the northern and southern edges of Pangaea as well as along the 0º latitude. These zones are shown in figure 7 which overlays them on maps of Pangaea.

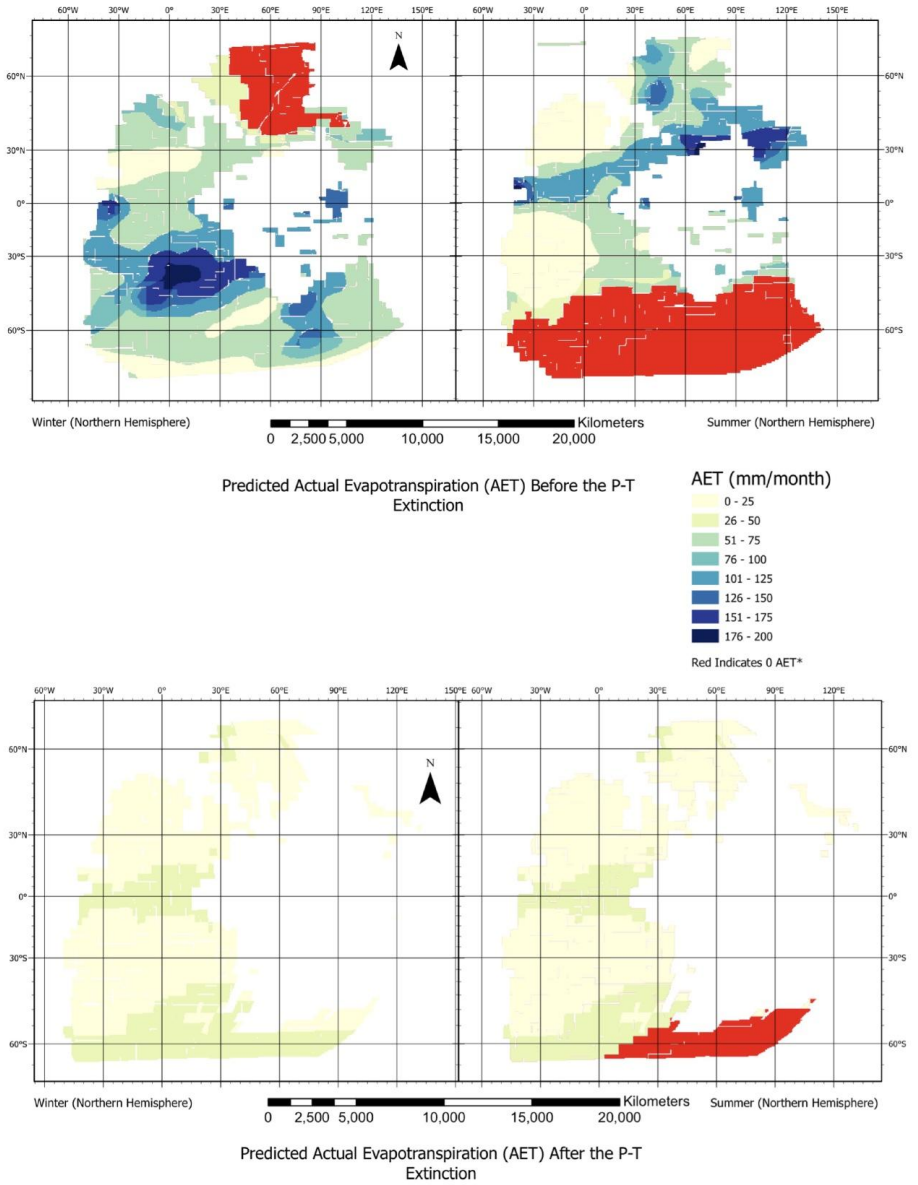

Figure 10 *Maps of predicted actual evapotranspiration values for Pangaea before (top) and after (bottom) the P-T extinction. Zones of red indicate areas where surface temperatures were negative and evapotranspiration was zero. The seasons are based on northern latitudes.*

When displayed spatially, there is clear zoning of increasing and decreasing evapotranspiration across Pangaea. The areas of low evapotranspiration values before the extinction saw increased values after the extinction. Likewise, the areas of larger values pre-extinction saw decreases in evapotranspiration after the extinction. These trends can be observed in figure 8. Notably, the decreases expressed as loss in millimeters per month were much larger than the values in the zones of increase.

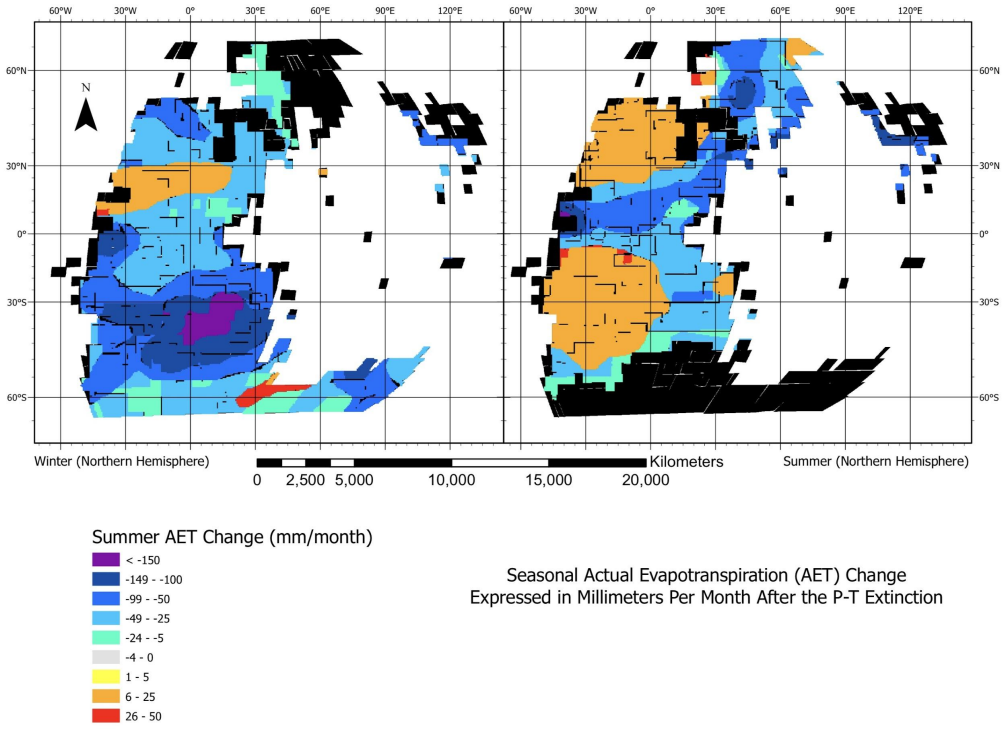

Figure 11 *Maps of change in actual evapotranspiration after the P-T extinction for northern latitude winter and summer. Change in AET is expressed as raw change in millimeters per month. Zones in black indicate areas where temperature zones were negative or where land mass assumptions from different studies did not overlap and are therefore undefined. Average loss across the continent was -36.8 mm/month.*

Greater evapotranspiration changes correlated with forested land cover types with two notable outliers. These correlations are shown in table 2. In this table it is observed that the evapotranspiration changes for pre-extinction forested land covers are typically concentrated below -65% reaching as extreme as -74.5% for the temperate evergreen forests. The only exception to this forest trend is the boreal conifer forest, which has the lowest change in evapotranspiration of any land cover type. The areas of non-forested land cover, savanna and desert, differed in their results. The savanna had

the second lowest change at -53.7%, only surpassing the boreal conifer at -30.7%. The desert on the other hand had the second most extreme change at -69.7%. Identical trends were noted for precipitation and have also been highlighted in table 2.

Table 2 *Pre-extinction values, raw changes, and percent changes in precipitation and actual evapotranspiration correlated to pre-extinction land cover types determined by Kutzbach & Ziegler (1993).*

Land Cover Type	Area (km^2)	Pre Extinction Precip. (mm/mon)	Precip. Change (mm/mon)	Precip. Change (%)	Pre Extinction AET (mm/mon)	AET Change (mm/mon)	AET Change (%)
Temperate Evergreen	3.99e7	91.2	-70.1	-76.9	76.6	-57.1	-74.5
Boreal Conifer	5.87e7	69.9	-32.2	-46.1	47.5	-14.6	-30.7
Tropical Rainforest	5.96e7	90.0	-60.8	-67.6	77.3	-50.6	-65.5
Tropical Deciduous	4.21e7	66.3	-45.0	-67.9	61.1	-40.2	-65.8
Temperate Deciduous	2.01e7	82.5	-56.3	-68.2	67.5	-45.7	-67.7
Savanna	6.58e6	45.7	-25.9	-56.7	41.7	-22.4	-53.7
Desert	1.50e7	40.3	-28.8	-71.5	38.3	-26.7	-69.7

3.1.2 Discharge and Mean Residence Time

The spatial distribution of discharge shows similar zonation to what was observed in evapotranspiration. The zones of discharge are mapped in figure 9. The winter zones appear almost identical to those observed for evapotranspiration, with the zones of lower values concentrated at the 30° North latitude and the southwestern portion of the continent and zones of higher values concentrated between the 0° and 60° South latitude. However, there is also a zone of high values at the north-east portion of Pangaea above the 30° latitude that was not observed in the evapotranspiration data. The summer zones show a similar phenomena where almost all zones for discharge are identical to those observed for evapotranspiration except for a large belt of high values located just south of a large area of low zones between the 30° and 60° South latitude.

Values for the post-extinction data were much more uniform, with the only outliers lying at the northern point of the continent in the winter and the southern point of the continent in the summer.

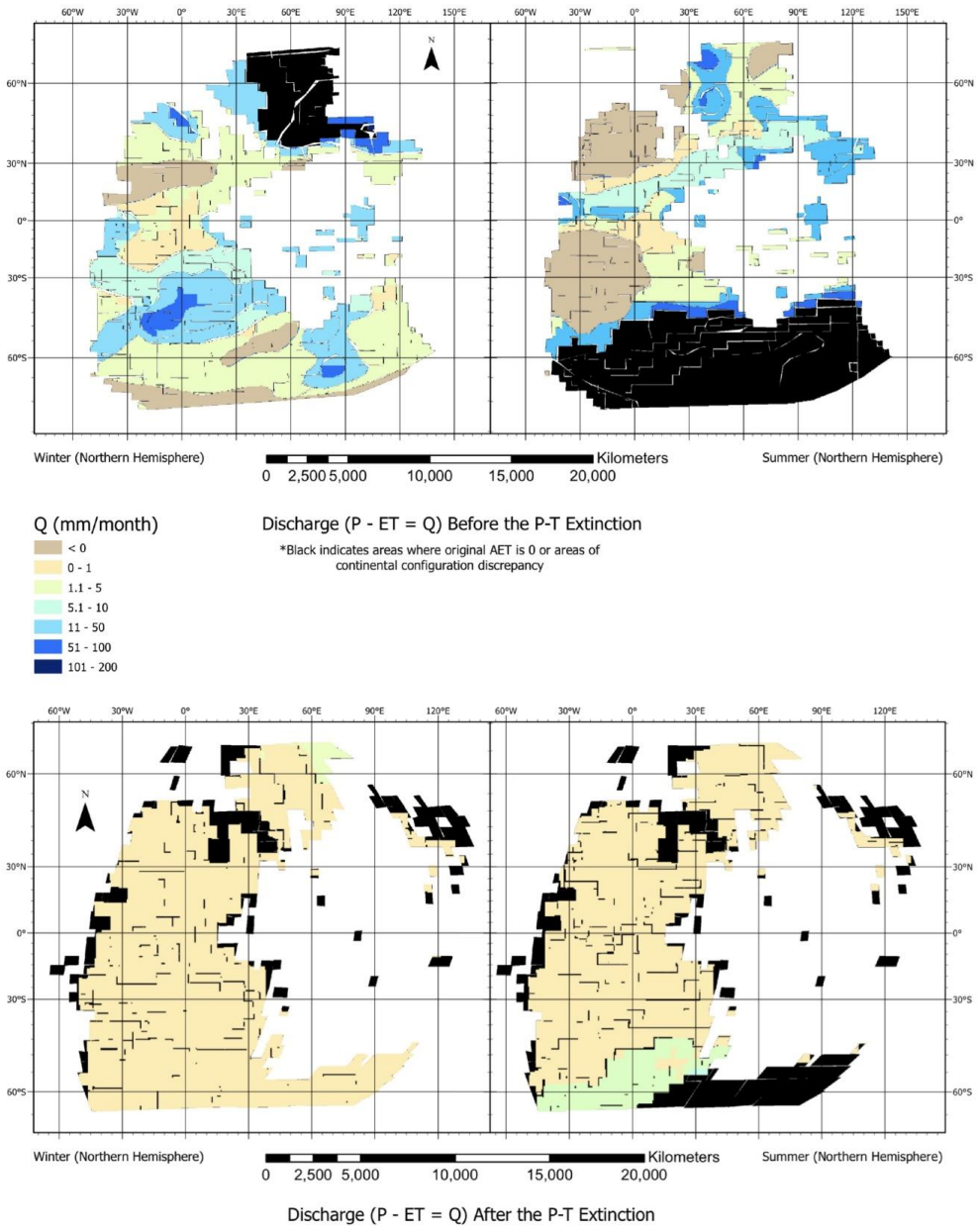

Figure 12 *Maps of predicted discharge values for Pangaea before (top) and after (bottom) the P-T extinction. Zones in black indicate areas where temperature zones were negative or where land mass assumptions from different studies did not overlap and are therefore undefined. The seasons are based on northern latitudes.*

The change in discharge follows similar patterns, with small patches of large change defining the global average. Overall the trends in this data set follow the trends observed in evapotranspiration change, with areas of low values pre-extinction seeing small increases, and areas of high values pre-extinction seeing larger decreases. As noted with the pre- and post-extinction discharge values, there are some differences in the zones which cause areas to be highlighted on the discharge change map shown in figure 10 that were not highlighted on the evapotranspiration change map.

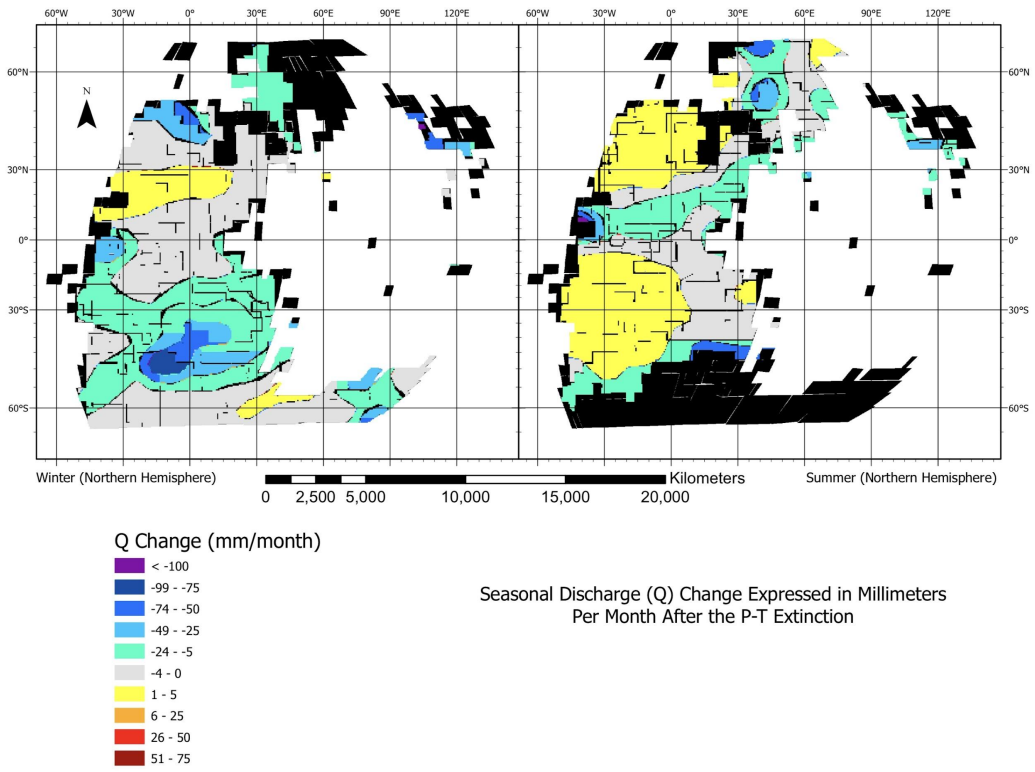

Figure 13 *Maps of change in discharge after the P-T extinction for northern latitude winter and summer. Change in discharge is expressed as raw change in millimeters per month. Zones in black indicate areas where temperature zones were negative or where land mass assumptions from different studies did not overlap and are therefore undefined. Average loss across the continent was -49.4 mm/month.*

The estimates of mean residence time before the P-T extinction show distinct zones unlike those seen in previous variables. As shown in figure 11, the pre-extinction zones of low values appear similar to all past variables. However, the zones of high values have in some cases drastically changed. In the summer, the east-west northern belt of high values appears fragmented, with zones of high values only being retained around the 60° East longitude and westward. The winter season sees an even more

unique set of zones as the primary zone of high values between the 30° and 60° South latitude has been lost. In its place are two smaller zones; one along the 60° South latitude in the central south of the continent, the other between the 30° and 60° South on the south-eastern tip of the continent. There is also a new zone of high values that stretches along the bottom of the zone of low values along the 30° North latitude.

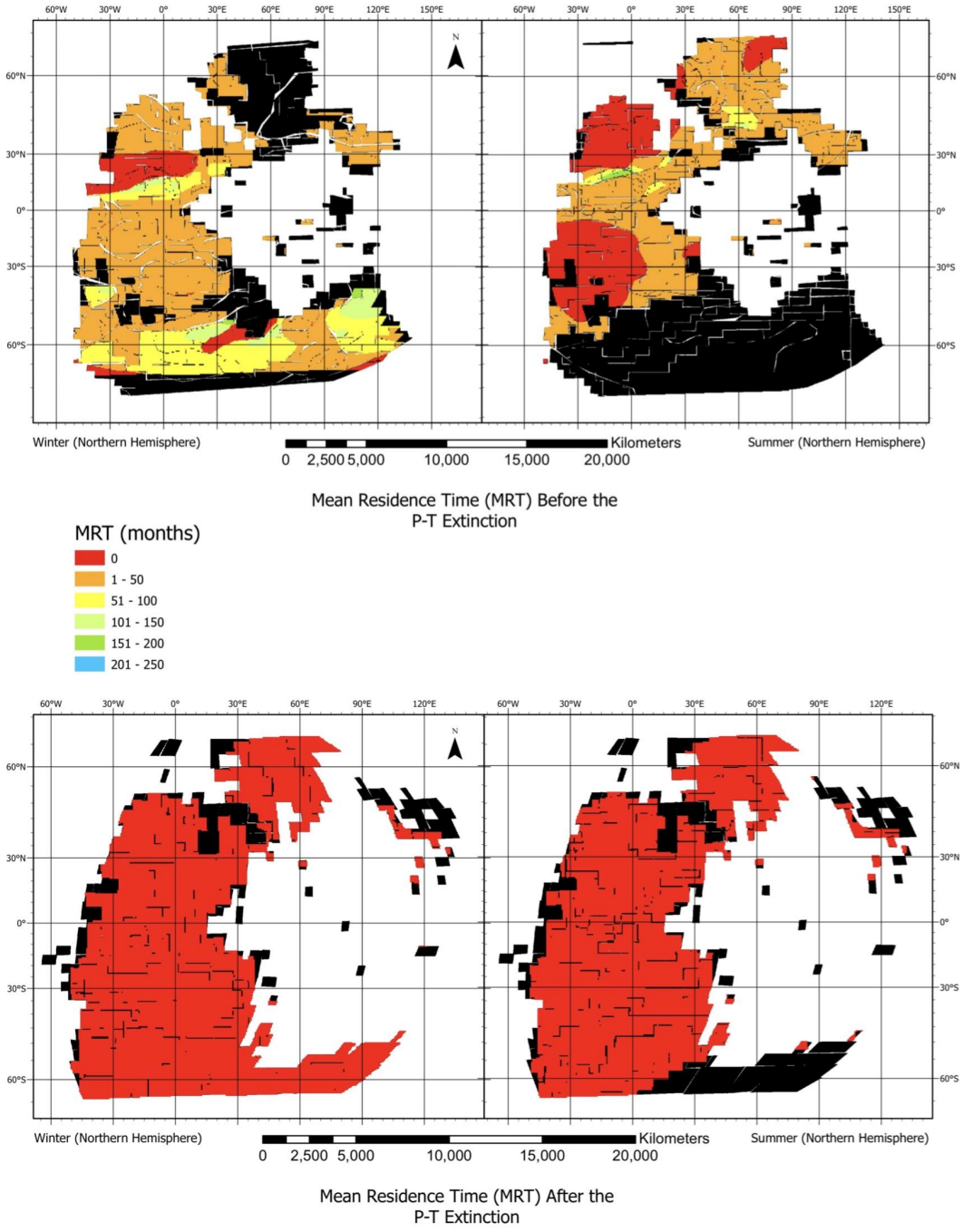

Figure 14 *Maps of predicted mean residence time (MRT) values for terrestrial water for Pangaea before (top) and after (bottom) the P-T extinction. Zones in black indicate areas where temperature zones were negative or where land mass assumptions from different studies did not overlap and are therefore undefined. The seasons are based on northern latitudes.*

Mean residence time decreases relatively uniformly across most of Pangaea when compared to the other variables. Unlike past variables, the zones of low values

before the extinction do not see any increase and blend in with the overall decrease across the maps in figure 12. The areas of high pre-extinction values continue to be highlighted, and show much higher amounts of decrease.

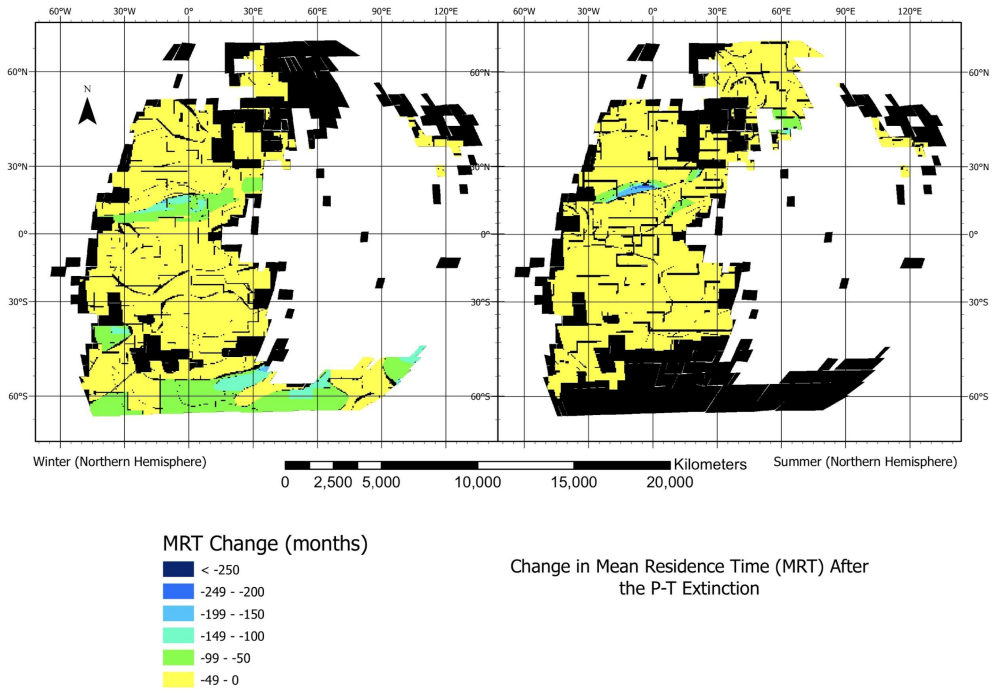

Figure 15 *Maps of change in mean residence time (MRT) of terrestrial water after the P-T extinction for northern latitude winter and summer. Change in MRT is expressed as raw change in millimeters per month. Zones in black indicate areas where temperature zones were negative or where land mass assumptions from different studies did not overlap and are therefore undefined. Average loss across the continent was -3.8 months.*

Comparing discharge and mean residence time to pre-extinction land cover type shows a significant change linked to all land cover types. As observed summarized in Table 3, there was a decrease in discharge ranging between -84% and -100% for all pre-extinction land cover types. There was no clear land cover factor that determined the greatest decrease, as two forested (one coniferous and one deciduous) and both non-forested land cover types saw a 100% decrease. Mean residence time changes, also highlighted in table 3, show much stronger land cover correlations. The pre-extinction forests all show decreases in mean residence time, with all but one decreasing by over 95%. The non-forested pre-extinction land covers both had a predicted pre-extinction mean residence time of 0 months and therefore on average saw no change after the extinction. The temperate conifer showed a change of -55%

which could be attributed to the zonal statistic calculation, registering some pre-extinction hotspots with no change seen in the desert and savanna biomes and high changes areas in the forested biomes. This would lead to an average change between 0 and -100% that is not accurate to the set conditions and should be considered a statistical outlier.

Table 3 *Pre-extinction values, raw changes, and percent changes in discharge and mean residence time of terrestrial water correlated to pre-extinction land cover types determined by Kutzbach & Ziegler (1993).*

Land Cover Type	Pre Extinction Q (mm/mon)	Q Change (mm/mon)	Q Change (%)	Pre Extinction MRT (months)	MRT Change (months)	MRT Change (%)
Temperate Evergreen	14.6	-16.5	-100	11	-6.1	-55.5**
Boreal Conifer	4.4	-3.7	-84.1	1.4	-1.4	-100
Tropical Rainforest	11.0	-9.3	-84.6	9.9	-10.1	-100
Tropical Deciduous	5.4	-4.9	-90.7	4.9	-4.8	-98.0
Temperate Deciduous	11.2	-11.9	-100	22.1	-21.3	-96.4
Savanna	3.4	-3.4	-100	0	0	0
Desert	2.2	-2.3	-100	0	0	0

** *The temperate evergreen bordered on areas with 0 pre-extinction mean residence time that were savanna or desert environments. This likely caused a shift in the average MRT percent change to lie between 0% and -100%.*

3.2 Sensible Heat

The spatial zones of increasing and decreasing latent heat flux correspond with the zones of increasing and decreasing evapotranspiration with some fragmentation and aggregation within the zones. As seen in figure 13, the outlines of the general zones of increase and decrease correlate with the zones of evapotranspiration change in figure 8. Within the zones in the winter there is less variation between the levels of decrease. The same is true for the areas of decrease for the summer and the inverse appears true for the areas of increase. The average loss in latent heat flux for the

continent of Pangaea was -2.1°C which is equivalent to a 2.1°C increase in sensible heat after the extinction.

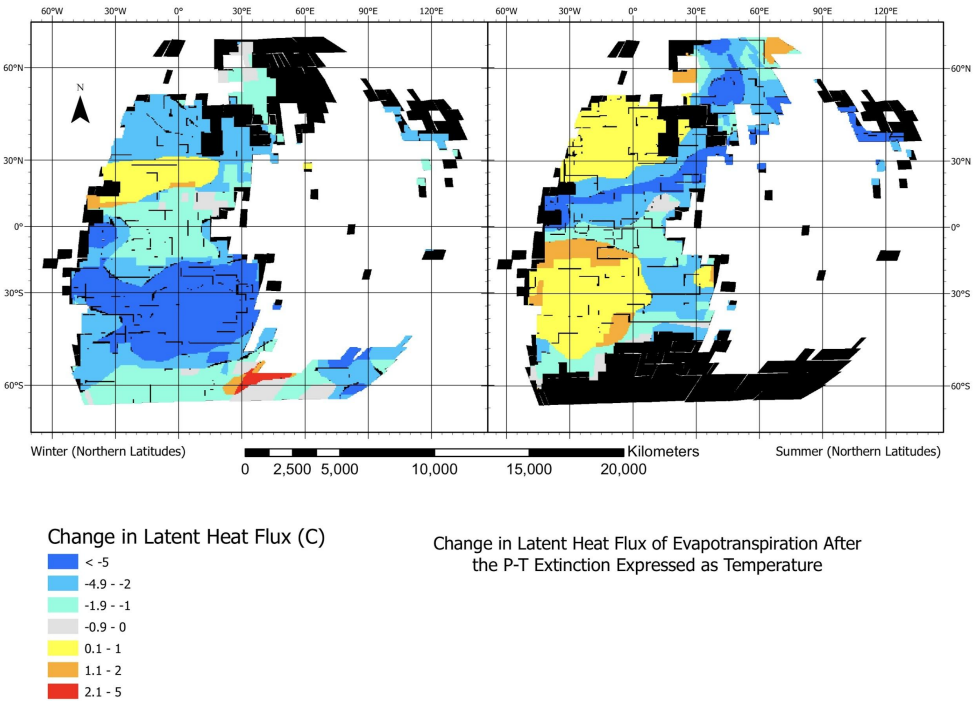

Figure 16 *Maps of change in latent heat flux after the P-T extinction for northern latitude winter and summer. Change in latent heat flux is expressed as temperature. Zones in black indicate areas where temperature zones were negative or where land mass assumptions from different studies did not overlap and are therefore undefined. Average loss across the continent was -2.1°C.*

When these values are inverted to sensible heat change and compared with land cover, a correlation becomes apparent. These observations are summarized in table 4. As with evapotranspiration and precipitation the greatest increase were mostly in the pre-extinction forest land covers ranging from 64.4% to 75.0%. The outlier again with forested land covers is the boreal conifer which shows the lowest sensible heat change at 33.3%. Savanna recorded the second lowest change at 54.2% while desert was much higher, sitting within the range of forested land covers at 68.1%.

Table 4 *Pre-extinction values, raw changes, and percent changes in sensible heat correlated to pre-extinction land cover types determined by Kutzbach & Ziegler (1993).*

Land Cover Type	Pre Extinction Sensible Heat (°C)	Change in Sensible Heat (°C)	Change in Sensible Heat (%)
Temperate Evergreen	4.4	3.3	75.0
Boreal Conifer	2.7	0.9	33.3
Tropical Rainforest	4.5	2.9	64.4
Tropical Deciduous	3.5	2.3	65.7
Temperate Deciduous	3.9	2.7	69.2
Savanna	2.4	1.3	54.2
Desert	2.2	1.5	68.1

4 Discussion

4.1 Water Balance

The results of the global water balances correspond with trends observed in present day studies of land cover and hydrology. General trends across the continent saw decreases in all water balance variables as well as mean residence time, supporting the first hypothesis of this study. These trends also support those observed in the literature review. The loss in evapotranspiration associated with the loss of Glossopteris forests matches similar studies in modern tropical region forests (Guimberteau et al., 2017). The decrease in all variables also supports a shift to a more arid climate suitable for the domination of herbaceous lycophytes at the start of the Triassic (Cook et al., 2012). When looking at specific land cover correlations we see that the most significant losses in discharge and mean residence time are associated with forested regions, signifying that the loss of forests may have contributed to more worsening arid conditions. This would match up with trends observed in studies of present day Mesoamerica (Cook et al., 2012). In general similar trends hold true for evapotranspiration but specific outliers must be analyzed more closely for the cause of discrepancies.

4.1.1 Actual Evapotranspiration

The change in evapotranspiration coupled with the associated change in precipitation have heavy implications on the availability of water just after the P-T extinction. On a global scale the reduction in precipitation and reduced evapotranspiration signifies that there was less available water entering the system, and less water being retained in a region to allow for evapotranspiration. This continues to support the aridity trends noted for general forest loss (Cook et al., 2012). However, when focusing down to the pre-extinction land cover scale two outliers were noted; the near polar boreal conifer forests, and the deserts of central Pangaea. The boreal conifer can be more easily explained in one of two ways. The first is simply an error in the data collection of this study. It should be noted that the areas where temperatures were negative before the P-T extinction led to undefined zones at different portions of the

map depending on the seasons. However, these undefined zones were always at the poles and it is therefore possible that many zones of boreal conifer were not properly observed as the data was unavailable. The other possible cause of this error is that, even though earth was in a greenhouse condition before and after the P-T extinction, there were still times where the poles would reach freezing temperatures which would have impacts on the seasonal water balance not captured using the assumptions this study made due to impacts of seasonal polar ice. The outlying nature of the desert is more bizarre as it lies in the center of the continent where the data appears the most sound. In this case however, the sources of the data may need to be brought into question. The last available study of global land cover of the late Permian was conducted in 1993, more than 20 years ago (Kutzbach & Ziegler, 1993). As with many elements of study in palaeoclimate and associated fields, even a decade can provide the time for a radical shift to change our understanding of the past. It may be possible then that since other input variables used in this study are more up to date, that the land cover generated by Kutzbach and Ziegler may no longer be an accurate picture of what Pangaea looked like at the time. Furthemore, the amounts of rainfall recorded by Kutzbach and Ziegler and used to generate land cover do not seem to correlate with the accepted precipitation rates of deserts as identified by the International Geosphere-Biosphere Programme. Despite these discrepancies, the predicted evapotranspiration data portrays a seemingly accurate picture of Pangaea's hydrology and has further implications for the terrestrial water systems.

4.1.2 Discharge and Mean Residence Time

Accounting for the decrease in available water, the coupled decrease in discharge and mean residence time can be easily supported. Despite observations of a link between forest loss and increased discharge (Guimberteau et al., 2017) the decrease in discharge after the amount of time in question can be easily explained and correlated to the fluvial system sedimentology. As seen in the previous section, there was a combined decrease in precipitation and evapotranspiration, signifying less available water. Therefore, despite the loss of forests which act as a means of increasing storage the total amount of discharge would need to decrease simply due to

there being less water entering the system than before the P-T extinction. However, the shift from meandering to braided fluvial systems seems to indicate an increase in discharge (War et al., 2000). When looking at the pre-extinction precipitation data there is clear evidence of seasonal heavy rainfall events (Kutzbach & Ziegler, 1993). Despite the lack of seasonal data post extinction, it can be assumed that this trend may have occurred it a similar fashion (albeit with less overall precipitation) given similar continental configurations (Chandra et al., 2021). Therefore, these shifts from low to high energy streams capture the intensity of major seasonal flooding events, which coupled with the loss of stabilizing forests, would have caused the full storm waters to be discharged. This results in an increased discharge for a portion of the year, while the general trend would shift towards the average decrease predicted in this study.

4.2 Sensible Heat

The results of the sensible heating component of this study suggest there may have been a correlation between the change in Pangaea's hydrology and the global increase in temperature. A 2021 study suggested that large igneous provinces such as the Siberian traps could not have been the single reason for the temperature increases seen at the P-T boundary (Park et al., 2021). Runaway greenhouse conditions and decreases in ozone have typically been used to supplement the Siberian trap hypothesis (Beerling, 2007). This study adds in another level to the temperature changing factors by adding in the sensible heat increase caused by the decrease in evapotranspiration. The results of this study suggest a possible global average increase of approximately 2^{o}C related exclusively to the decreased evapotranspiration. This would account for roughly 20% of 10^{o}C change in global temperature predicted at the P-T boundary (Scotese et al., 2021), and supports the second hypothesis of this thesis. Furthermore, this supports the Siberian trap hypothesis by lending another stepping stone to the sequence of global heating. It is important to note that the loss of the ozone layer at the P-T extinction would have led to further modifications of the terrestrial energy balance than what was shown by examining the sensible heat change from evapotranspiration change alone. However, without knowing the general changes in

radiation entering the system these differences cannot be applied to the 2^{o}C result of this study.

5 Conclusion

The results of this study show the first estimates of many water balance variables for the P-T extinction. In support of the first hypothesis of this thesis there was a global decrease in precipitation, evapotranspiration, discharge, and mean residence time of terrestrial water. The changes found for evapotranspiration, discharge, and MRT are the first of their kind for the P-T extinction and support theories and observations that are already known for this period of history. The second hypothesis is supported by the results of the sensible heat data which suggests that approximately 2^{o}C of the global warming during the P-T extinction may have been due to the loss of global evapotranspiration leading to increased terrestrial warming. There are limitations to these results however. The input data sets for this study come from different times, some multiple decades apart. This means that some of the input data sets may not be as valid as others and attempts should be made to bring these variables into more modern light. This is especially true for land cover maps, which have not been compiled for Pangaea in over 25 years since the time of this study (Kutzbach & Ziegler, 1993). Furthermore, the time gaps between studies also meant that Pangaea's configuration was not uniform across all studies, leading to zones of undefined data in this study. Ideally future studies would balance and quantify these input variables on a uniform continental configuration, to allow the most accurate assessment of global spatial trends.

The data this study provides can be useful in our understanding of both palaeoclimate modeling and future climate predictions. The general decrease in available water shows that terrestrial systems were no longer able to support the growth of the glossopteris forests after their loss, and new specialized plants would need to take hold of the now much more arid environments. This perfectly lays the foundation for the domination of lycophytes after the P-T extinction that has been observed in multiple regions (Feng et al., 2020). It would also help create an extreme environment more hostile to the animals that had evolved to thrive in the once productive forest ecosystems, pushing towards a terrestrial extinction rate observed in the P-T extinction (Erwin, 1994). It also adds another piece to the sequence of events leading to the

known temperature spike at the P-T boundary when combined with other events such as the Siberian traps and the build of atmospheric carbon (Burgess et al., 2007). These results also relate to the present issue of deforestation. As more areas of forest are converted into barren or agricultural surfaces where storage of water is greatly reduced, smaller scale regional trends in water balance loss have become highlighted in various regions (Guimberteau et al., 2017). These results show a worst case example of forest loss, while also acting to use this extreme case to highlight the trends that occur in modern settings.

6 References

Ahmadi S.H., Fooladmand H.R. 2008. Spatially distributed monthly reference evapotranspiration derived from the calibration of the Thornthwaite equation: a case study, south of Iran. Irrigation Science. 26: 303-312. https://doi.org/10.1007/s00271-007-0094-8

Allen R.G., Pereira L.S., Raes D., Smith M. 1998. Crop evapotranspiration: guidelines for computing crop requirements. FAO Irrigation and Drainage Paper No. 56. FAO, Rome, Italy.

Arnold J.G., Srinivasan R., Muttiah R.S., Williams J.R. 1998. Large area hydrologic modeling and assessment part I: model development. Journal of the American Water Resources Association. 34(1): 73-89.

Augstein F., Carlsbecker A. 2018. Getting to the roots: a developmental view of root anatomy and function from arabidopsis to lycophytes. Frontiers in Plant Science. 25. https://doi.org/10.3389/fpls.2018.01410

Beerling D. 2007. An ancient ozone catastrophe. In, The emerald planet: how plants changed earth's history. Oxford University Press, New York. pp. 61-86.

Black B.A., Lamarque J., Shields C.A., Elkins-Tanton L.T., Kiehl J.T. 2014. Acid rain and ozone depletion from pulsed siberian traps magmatism. Geology. https://doi.org/10.1130/G34875.1

Brand U., Blamey N., Garbelli C., Griesshaber E., Posenato R., Angiolini L., Azmy K., Farabegoli E., Came R. 2016. Methane hydrate: killer cause of earth's greatest mass extinction. Palaeoworld. 25(4): 496-507. https://doi.org/10.1016/j.palwor.2016.06.002

Buatois L.A., Borruel-Abadía V., De La Horr R., Galán-Abellán A.B., López-Gómez J., Barrenechea J.F., Arche A. 2021. Impacts of permian mass extinctions on continental invertebrate infauna. Terra Nova. 33(5): 455-464. https://doi.org/10.1111/ter.12530

Budyko M.I. 1974. Climate and life. New York: Academic Press.

Burgess S.D., Muirhead J.D., Bowring S.A. 2017. Initial pulse of siberian traps sills as the trigger of the end-permian mass extinction. Nature Communications. 8(164). https://doi.org/10.1038/s41467-017-00083-9

Cascales-Miñana B., Diez J.B., Gerrienne P., Cleal C.J. 2015. A palaeobotanical perspective on the great end-permian biotic crisis. International Journal of Paleobiology. 28(8). https://doi.org/10.1080/08912963.2015.1103237

Chandra R., Cripps S., Butterworth N., Muller R.D. 2021. Precipitation reconstruction from climate-sensitive lithologies using bayesian machine learning. Environmental Modelling & Software. 139. https://doi.org/10.1016/j.envsoft.2021.105002

Cook B.I., Anchukaitis K.J., Kaplan J.O., Puma M.J., Kelly M., & Gueyffier D. 2012. Pre-columbian deforestation as an amplifier of drought in mesoamerica. Geophysical Research Letters. 39(16). https://doi.org/10.1029/2012GL052565

Creed I.F., Spargo A.T., Julia J.A., Buttle J.M., Adams M.B., Beall F.D., Booth E.G., Campbell J.L., Clow D., Elder K., et al. 2014. Changing forest water yields in responses to climate warming: results from long-term experimental watershed sites across North America. Global Change Biology. 20: 3191-3208. https://doi.org/10.1111.gcb.12615

Cui Y., Li M., van Soelen E.E., Peterse F., Kürschner W.M. 2021. Massive and rapid predominantly volcanic CO2 emission during the end-Permian mass extinction. Proceedings of the National Academy of the United States of America. 118(37): e2014701118. https://doi.org/10.1073/pnas.2014701118

Davydov V.I., Karasev E.V., Nurgalieva N.G., Schmitz M.D., Budnikov I.V., Biakov A.S., Kuzina D.M., Silantiev V.V., Urazaeva M.N., Zharinova V.V., Zorina S.O., Gareev B., Vasilenko D.V. 2021. Climate and biotic evolution during the Permian-Triassic transition in the temperate northern hemisphere, kutnetsk basin, Siberia, Russia. Palaeogeography, Palaeoclimatology, Palaeoecology. 573. https://doi.org/10.1016/J.palaeo.2021.110432

Delevoryas T. Gould R.E. 1977. The biology of glossopteris: evidence from petrified seed-bearing and pollen-bearing organs. Alcheringa. 1(4): 387-399. https://doi.org/10.1080/03115517708527774

Denning S. (n.d.). Surface Energy Budget. AT761 Land-Atmosphere Interaction. CSU ATS.

Erwin D.H. 1994. The permo-triassic extinction. Nature. 367: 231-236. https://doi.org/10.1038/367231a0

Falkenmark M., Rockström J. 2006. The new blue and green water paradigm: breaking new ground for water resources planning and management. Journal of Water Resources Planning and Management. 132(3): 129-132. https://doi.org/10.1061/(ASCE)0733-9496(2006)132:3(129)

Faramarzi M., Abbaspour K.C., Schulin R., Yang H. 2009. Modeling blue and green water resources availability in iran. Hydrological Processes. 23: 486-501. https://doi.org/10.1002/hyp.7160

Feng Z., Wei H., Guo Y., He X., Sui Q., Zhou Y., Liu H., Gou X., Lv Y. 2020. From rainforest to herbland: new insights into land plant responses to the end-Permian mass extinction. Earth-Science Reviews. 204. https://doi.org/10.1016/j.earthscirev.2020.103153

Frank T.D., Fielding C.R., Winguth A.M.E., Savatic K., Tevyaw A., Winguth C., McLoughlin S., Vajda V., Mays C., Nicoll R., Boeking M., Crowley JL. 2021. Pace, magnitude, and nature of terrestrial climate change through the end-Permian extinction in southeastern Gondwana. Geology. 20(20). https://doi.org/10.1130/G48795.1

Guimberteau M., Ciais P., Ducharne A., Boisier J.P., Aguiar A.P.D., Biemans H., Deurwaerder H.D., Galbraith D., Kruijit B., Langerwisch F., Poveda G., Rammig A., Rodriguez D.A., Tejada. Thonicke K., von Randow C., von Randow RCS., Zhang K., Verbeeck H. 2017. Impacts of future deforestation and climate change on the hydrology of the Amazon basin: a multi-model analysis with a new set of land-cover change scenarios. Hydrology and Earth System Science. 21: 1455-1475. https://doi.org/10.5194/hess-21-1455-2017

Harper C.J., Taylor T.N., Krings M. Taylor E.L. 2013. Mycorrhizal symbiosis in the paleozoic seed fern glossopteris from antarctica. Review of Palaeobotany and Palynology. 192: 22-31. https://dx.doi.org/10.1016/j.revpalbo.2013.01.002

Hochuli P.A., Hermann E., Vigran J.O., Bucher H., Weissert H. 2020. Rapid demise and recovery of plant ecosystems across the end-Permian extinction event. Global and Planetary Change. 74: 144-155. https://doi.org/10.1016/j.gloplacha.2010.10.004

Hu X., Næss J.S., Iordan C.M., Huang B., Zhao W., Cherubini F. 2021. Recent global land cover dynamics and implications for soil erosion and carbon losses from deforestation. Anthropocene. 34. https://doi.org/10.1016/j.ancene.2021.100291

Kauffman S., Droogers P., Hunink J., Mwaniki B., Muchena F., Gicheru P., Bindraban P., Onduru D., Cleveringa R., Bouma J. 2014. Green water credits - exploring its potential to enhance ecosystem services by reducing soil erosion in the upper tana basin, Kenya. International Journal of Biodiversity Science, Ecosystem Services & Management. 10(2):133-143. https://doi.org/10.1080/21513732.2014.890670.

Kiehl J.T., Shields C.A. 2005. Climate simulation of the latest permian: implications for mass extinction. Geology. 33(9): 757-760. https://doi.org/10.1130/G21654.1

Kutzbach J.E., Ziegler A.M. 1993. Simulation of late permian climate and biomes with an atmosphere-ocean model: comparisons with observations. Philosophical Transactions of the Royal Society of London B. 341: 327-340.

Lhomme J., Moussa R. 2016. Matching the budyko functions with the complementary evaporation relationship: consequences for the drying power of the air and the priestly-taylor coefficient. Hydrology and Earth System Sciences. 20: 4857-4865. https://doi.org/10.5194/hess-20-4857-2016

Liao W., Liu X., Burakowski E., Wang D., Wang L., Li D. 2020. Sensitivities and responses of land surface temperature to deforestation-induced biophysical changes in two global earth system models. Journal of Climate. 33(19): 8381-8399. https://doi.org/10.1175/JCLI-D-19-0725.1

Mays C., Vajda V., Frank T.D., Fielding C.R., Nicoll R.S., Tevyaw A.P., McLoughlin S. 2020. Refined permian-triassic floristic timeline reveals early collapse and delayed recovery of south polar terrestrial ecosystems. GSA Bulletin. 132(7-8): 1489-1513. https://doi.org/10.1130/B35355.1

McLoughlin S. 2011. Glossopteris - insights into the architecture and relationships of an iconic permian gondwanan plant. Journal of the Botanical Society of Bengal. 65(2): 93-106

Miller M.F., Knepprath N.E., Cantrill D.J., Francis J.E., Isabelle J.L. 2016. Highly productive polar forests from the permian of antarctica. Palaeogeography, Palaeoclimatology, Palaeoecology. 441(2): 292-304. https://doi.org/10.1016/j.palaeo.2015.06.016

Mills B.J.W., Donnadieu Y., Goddéris Y., 2021. Spatial continuous integration of Phanerozoic global biogeochemistry and climate. Gondwana Research. https://doi.org/10.1016/j.gr.2021.02.011

Moeletsi M.E., Walker S., Hamandawana H. 2013. Comparison of the Hargreaves and samani equation and the Thornthwaite equation for estimating dekadal evapotranspiration in the free state province, South Africa. Physics and Chemistry of the Earth, Parts A/B/C. 66: 4-15. https://doi.org/10.1016/j.pce.2013.08.003

Neish P.G., Drinnan A.N., Cantrill D.J. 1993. Structure and ontogeny of vertebraria from silicified permian sediments in east antarctica. Review of Palaeobotany and Palynology. 79: 221-244.

Nijzink R.C., Schymanski S.J. 2022. Vegetation optimality explains the convergence of catchments on the Budyko curve. Hydrology and Earth System Sciences. https://doi.org/10.5194/hess-2022-97

Nobre P., Malagutti M., Urbano D.F., de Almeida R.A.F., Giarolla E. 2009. Amazon deforestation and climate change in a coupled model simulation. Journal of Climate. 22(21): 5686-5697. https://doi.org/10.1175/2009JCLI2757.1

Oda T., Egusa T., Ohte N., Hotta N., Tanaka N., Green M.B., Suzuki M. 2021. Effects of changes in canopy interception on stream runoff response and recovery following clear-cutting of a japanese coniferous forest in fukuroyamas awa experimental watershed. Hydrological Processes. 35: e14177. https://doi.org/10.1002/hyp.14177

Park Y., Swanson-Hysell N.L., Lisiecki L.E., MacDonald F.A. 2021. Evaluating the relationship between the area and latitude of large igneous provinces and earth's long term climate state. Large Igneous Provinces: A Driver of Global Environmental and Biotic Changes, Geophysical Monograph 225, First Edition. https://doi.org/10.1002/9781119507444.ch7

Payne J.L., Kump L.R. 2007. Evidence for early triassic massive volcanism from quantitative interpretation of carbon isotope fluctuations. Earth and Planetary Science Letters. 256(1-2): 264-277. https://doi.org/10.1016/j.epsl.2007.01.034

Saitoh M., Isozaki Y. 2020. Carbon isotope chemostratigraphy across the Permian-Triassic boundary at chaotian, China: implications for the global methane cycle in the aftermath of the extinction. Frontiers in Earth Science. 8(596178). https://doi.org/10.3389/feart.2020.596178

Schuol J., Abbaspour K.C., Yang H., Srinivasan R., Zehnder A.J.B. 2008. Modeling blue and green water availability in africa. Water Resources Research. 44(7). https://doi.org/10.1029/2007WR006609

Schyns J.F., Hoekstra A.Y., Booij M.J. 2015. Review and classification of indicators of green water availability and scarcity. Hydrology and Earth System Sciences. 19: 4581-4608. https://doi.org/10.5194/hess-19/4581/2015

Scotese C.R., Song H., Mills B.JW., van der Meer D.G. 2021. Phanerozoic paleotemperatures: the earth's changing climate during the last 540 million years. Earth-Science Reviews. https://doi.org/10.1038/srep04132

Song H., Wignall P.B., Chu D., Tong J., Sun Y., Song H., He W., Tian L. 2014. Anoxia/high temperature double whammy during the permian-triassic marine crisis and its aftermath. Scientific Reports. 4(4132). https://doi.org/10.1038/srep04132

Sterling S.M. 2019. New perspectives on the history of the global water cycle: lessons from the past to better prepare for our future. Catchment Science: Interactions of Hydrology, Biology and Geochemistry

Sterling S.M., Ducharne A., Polcher J. 2013. The impact of global land-cover change on the terrestrial water cycle. Nature Climate Change. 3: 385-390. https://doi.org/10.1038/NCLIMATE1690

Stevens L.G., Hilton J. Bond D.P.G., Glasspool I.J., Jardine P.E. 2011. Radiation and extinction patterns in permian floras from north china as indicators for environmental and climate change. Journal of the Geological Society, London. 168: 607-619. https://doi.org/10.1144/0016-76492010-042

Thornthwaite C.W. 1948. An approach toward a rational classification of climate. Geographical Review. 38(1): 55-94. https://doi.org/10.2307/210739

Ward P.D., Montgomery D.R., Smith R. 2000. Altered river morphology in South Africa related to the Permian-Triassic extinction. Science. 289(5485): 1740-1743. https://doi.org/10.1126/science.289.5485.1740

Wu H., Zhang S., Hinnov L.A., Jiang G., Feng Q., Li H., Yang T. 2013. Time-calibrated milankovitch cycles for the late permian. Nature Communications. 4: 2452. https://doi.org/10.1038/ncomms3452

Wu J., Deng G., Zhou D., Zhu X., Ma J., Cen G., Jin Y., Zhang J. 2021. Effects of climate change and land-use changes on spatiotemporal distributions of blue and green water in ningxia, northwest china. Journal of Arid Land. 13(7): 674-687. https://doi.org/10.1007/s40333-021-0074-5

Wu Y., Chu D., Tong J., Song H., Corso J.D., Wignall P.B., Song H., Du Y., Cui Y. 2021. Six-fold increase of atmospheric pCO2 during the permian-triassic mass extinction. Nature Communications. 12: 2137. https://doi.org/10.1038/s41467-021-22298-7

Zhu Z., Liu Y., Kuang H., Benton M.J., Newell A.J., Xu H., An W., Ji S., Xu S., Peng N., Zhai Q. 2019. Altered fluvial patterns in north China indicate rapid climate change linked to the Permian-Triassic mass extinction. Scientific Reports. 9(16818). https://doi.org/10.1038/s41598-019-53321-z

7 Appendices

7.1 Literature Review Description and Search Strategy

The majority of this review will focus on present understanding of the P-T extinction, with some focus on present day climate studies to highlight key hydrological concepts. Research on the P-T extinction will predominantly focus on how the event impacted the global climate, vegetation, and fluvial systems. Research in this category will be contained within the 2000s to ensure that current understanding of the extinction is held, while also accounting for some separate viewpoints. The studies in present day settings with focus on water balance and its association with forest loss. To link these two topics, the concept of green water will be implemented in this study. Studies specifically discussing green water are typically more recent, however the older studies discussing similar ideas will be covered to allow a broad range of data availability. In both topics, an overview of the current understanding will be provided along with an analysis of some methods of modeling. Furthermore, studies that carry the same or similar theses will be used for multiple regions or geologic formations from different countries to show global trends. After discussing the literature compiled in this study, the knowledge gaps will be summarized at the end of the review.

To find the background information and data for this study the ProQuest GeoRef database was used with support from the Dalhousie library link search parameter in Google Scholar. Results for all searches were filtered to journal entries and newer papers were selected preferentially to ensure numbers and findings were up to date. General terms that were consistent across almost all searches included “green water”, “climate”, and “deforestation”. When searching for data specific to the time period of interest, or processes occurring at that time, terms including “Permian-Triassic extinction”, “Glossopteris”, and/or “Lycophytes” were included. Search terms which pertained to stores of water that were impacted during the extinction and included “rivers” and “fluvial”. The final set of search terms focused on major data points that

needed to be collected, including “evapotranspiration”, “precipitation”, and “soil moisture”, and/or “root zone”.

7.2 Potential Evapotranspiration

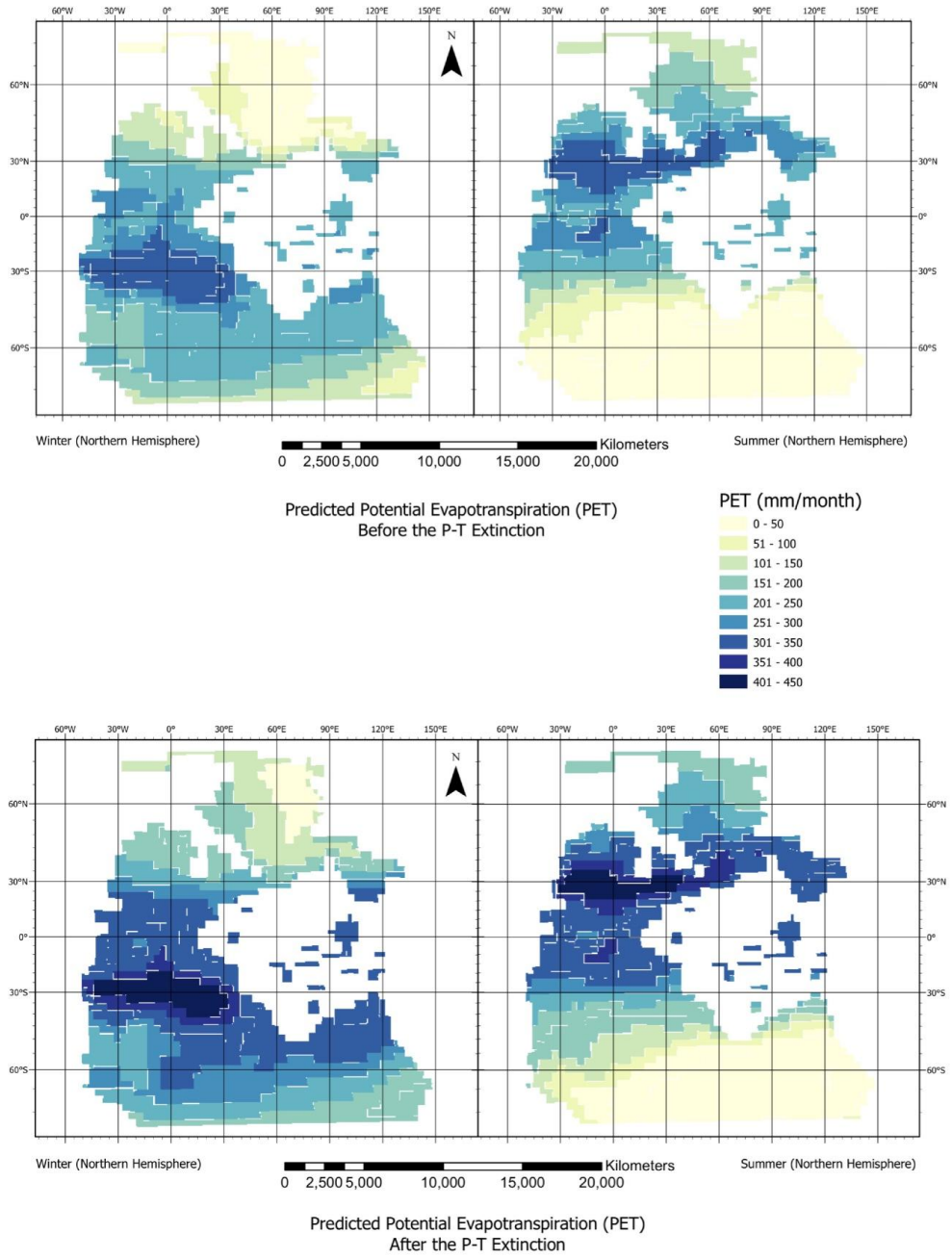

Figure A1 Maps of predicted potential evapotranspiration values for Pangaea before (top) and after (bottom) the P-T extinction. The seasons are based on northern latitudes.

7.3 Dryness

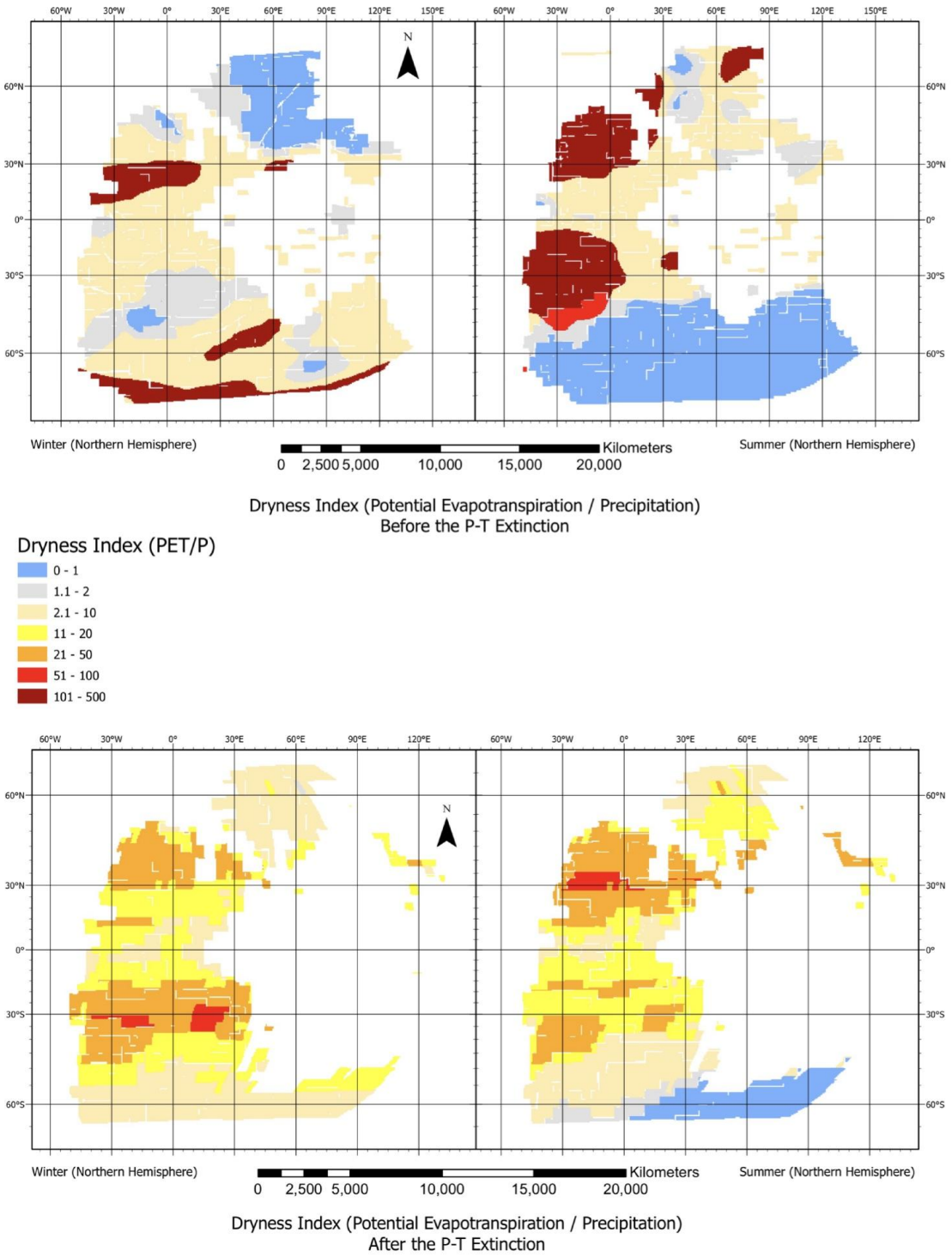

Figure A2 Maps of predicted dryness values for Pangaea before (top) and after (bottom) the P-T extinction. The seasons are based on northern latitudes.

7.4 Latent Heat Flux as Energy

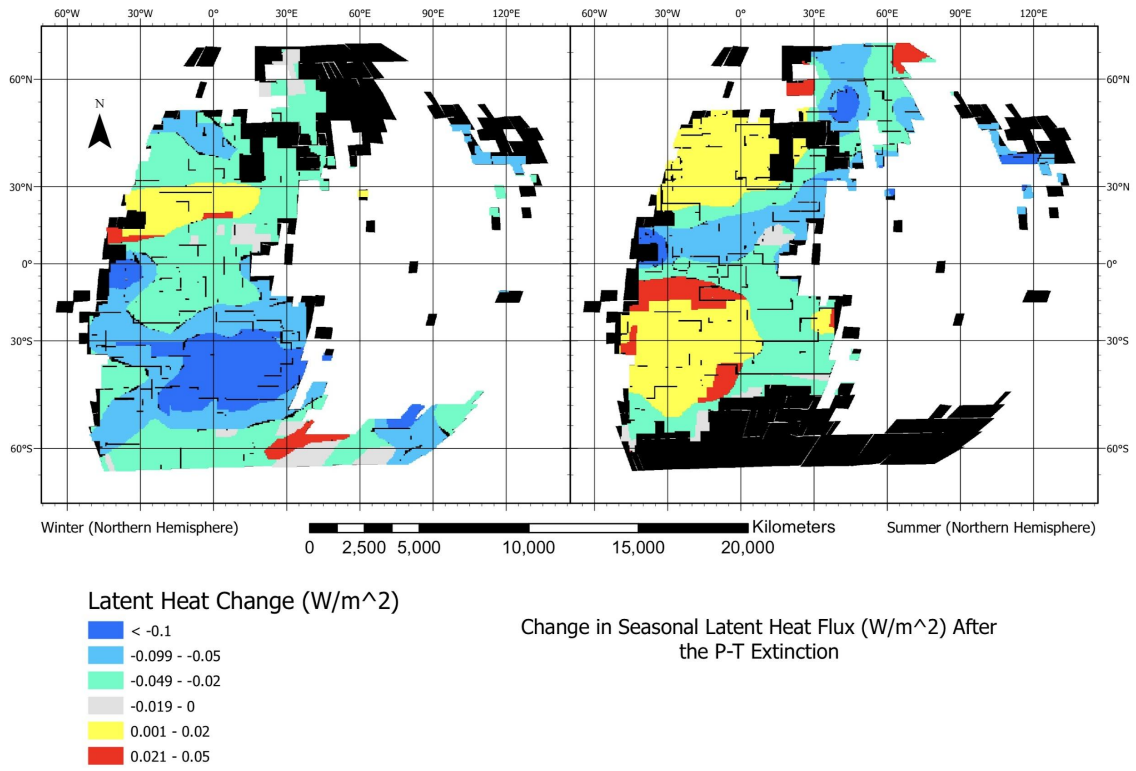

Figure A3 Maps of change in latent heat flux after the P-T extinction for northern latitude winter and summer. Change in latent heat flux is expressed as energy. Zones in black indicate areas where temperature zones were negative or where land mass assumptions from different studies did not overlap and are therefore undefined.